Fluid Dynamics, Pattern Formation

Michael Bestehorn
Brandenburg University of Technology, Cottbus, Germany

Article Outline

Glossary

Order parameter(s) (Field) variable(s) characterizing the spatio-temporal state of a system. Other state variables such as velocity, temperature, density, etc. can be computed if the order parameter(s) are known.

Control parameter(s) Parameters which are fixed and can be tuned from outside of the system under consideration.

Critical point, threshold, onset The points in control parameter space where new and qualitatively different solutions bifurcate from (usually simpler) ones.

Slaving principle Stated by H. Haken in 1975, the slaving principle allows for a huge reduction of degrees of freedom close to a critical point. It states that a very large number of linearly damped modes are slaved to and therefore completely determined by the few modes that grow in the vicinity of the critical point. The amplitudes of the growing modes are also called order parameters.

Natural patterns Spatial patterns showing a certain periodic (near) order, but also defects, grain boundaries etc.

Turing patterns Natural patterns that have a certain typical length scale and that show relaxation to a stationary state in the long term. Typical ingredients of Turing patterns are stripes, hexagons and squares.

Swift–Hohenberg equation Derived by Swift and Hohenberg in 1977 and nowadays established as the standard form for a scalar, real-valued order parameter equation showing Turing patterns at onset.

Coarsening The monotonic increase of the typical length scale of a structure in time. Often connected to spinodal decomposition, for example, of a binary mixture of non-mixing components such as water and oil. Small oil droplets in the beginning merge and finally form a large oil drop on the water surface. Coarsening slows down if the length scale increases.

Definition of the Subject

The state of a fluid is described by its velocity, density, pressure, and temperature. All these variables depend in general on space and time. Pattern formation refers to the situation where one or more of these variables are organized within a certain spatial and/or temporal order. This order has macroscopic length and time scales, that is, characteristic lengths and times are much larger than those of the atoms or molecules which constitute the fluid. Therefore a continuous description is appropriate.

Macroscopic fluid patterns may be encountered in nature as well as in technological applications for a large variety of different systems. Far from being complete, we mention some examples:

A. Hutt, H. Haken (eds.), *Synergetics*,
https://doi.org/10.1007/978-1-0716-0421-2_214

Originally published in
R. A. Meyers (ed.), *Encyclopedia of Complexity and Systems Science*, © Springer-Verlag 2009
https://doi.org/10.1007/978-3-642-27737-5_214

- Water waves caused by wind or by sea quakes and land slides (Tsunamis).
- Localized excitations of the surface of a fluid (solitons), such as that seen on shallow water channels.
- Shear instabilities in clouds or in multi-layer systems such as the Kelvin–Helmholtz instability or the Rayleigh–Taylor-instability.
- Surface deflections in the form of holes or drops of thin fluid films in coating or wetting processes.
- Convection instabilities in laboratory experiments, but also in the atmosphere, in the earth's interior or in stars.
- Creation and controlled growth of ordered structures in (nano-) technological applications.
- Biological applications: Behavior of liquid films on leaves or of the tear film on the cornea of the eye. Dynamics of thin blood layers, blood clotting.
- Films on the walls of combustion cells.
- Lubrication films in mechanical machines.

Fluid patterns may occur due to several mechanisms. One can distinguish between two main cases: Patterns excited and organized by some external forces or disturbances (such as Tsunamis) and those formed by instabilities. The latter may show the aspects of self-organization and will be the focus of the present contribution.

Introduction

Since the first observations of Michael Faraday almost 180 years ago (Faraday 1831) (Fig. 1), pattern formation in liquids or gases (*fluids*) has been subject to innumerable experimental (Bodenschatz et al. 2000; Schatz and Neitzel 2001; Van Dyke 1982), theoretical (Chandrasekhar 1961; Colinet et al. 2001; Getling 1998) and, later on, numerical work (Bestehorn 1993; Busse 1989; Pesch 1996). After the famous experiments by Henri Bénard around 1901 (Bénard 1901), convection in a single or later in multi-component fluids came into the focus of interest. The first theoretical studies were made by Lord Rayleigh (Lord 1915). Theoretical computations up to the early 1960s were restricted on the linearized basic equations and could explain the existence of critical points in parameter space as well as the observed length scales of the structures found experimentally (Block 1956; Palm 1960). In the meantime, Alan Turing (Turing 1952) showed in his famous paper of 1952 that similar patterns could emerge out of equilibrium in reaction-diffusion systems. It took almost 40 years for an experimental confirmation using the so-called CIMA reaction (Castets et al. 1990; Ouyang and Swinney 1991).

With the appearance and rapid development of computers, the field gained further momentum from the new discipline of nonlinear dynamics

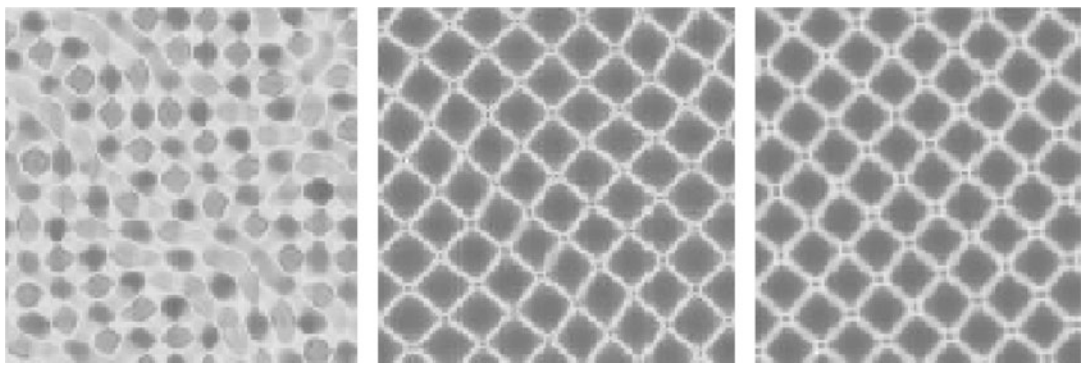

Fluid Dynamics, Pattern Formation, Fig. 1 Michael Faraday observed surface patterns on a liquid horizontal layer if the whole layer vibrated vertically with a certain amplitude and frequency. Very often, regular squares are found, as shown in the time series as a numerical result of the shallow water equations (see Section "Surface Waves")

and nonlinear system theory (Argyris et al. 1994; Guckenheimer and Holmes 2002; Haken 1975, 2004). Early computations in 1963 by Edward Lorenz of a system of three coupled ordinary differential equations derived by a crudely truncated mode expansion of the Navier–Stokes equations revealed the first chaotic attractor of a dissipative system (Lorenz 1963). Though the chaotic behavior seen in the Lorenz equations does not originate from hydrodynamic equations and has nothing to do with irregular fluid behavior, the Lorenz model now stands on its own as a paradigm for a relatively simple system showing low dimensional chaos (Sparrow 1982).

Patterns that emerge from an instability roughly pass through two phases. As long as amplitudes (or order parameters) are small, the behavior is often determined by the linear parts of the system and exponential growth of a certain part of the mode spectrum is found. In the second phase, nonlinearities come into play and may lead to saturation and selection of certain mode configurations, seen then as regular structures in configuration space (Fig. 2). The full mathematical description of hydrodynamic systems has been well known for a long time. Fluid motion is described by the Euler or Navier–Stokes equations, temperature fields by the heat equation and chemical concentrations by some nonlinear reaction-diffusion equations. The location and spatio-temporal evolution of surfaces or interfaces can be computed by the kinematic boundary conditions if the velocity of the fluid near the interface is known. All these equations can be coupled and provided with suitable boundary and initial conditions, resulting in rather complicated systems of nonlinear partial differential equations. Even today in the age of supercomputers, their further treatment, especially in three spatial dimensions, remains a challenge.

On the other hand, directly solving the basic equations, can be considered merely as another experiment. For these reasons and to get a deeper insight into the physics behind pattern formation, other methods have been devised. Very often one of the three spatial dimension is distinguished, either for physical reasons or simply due to the geometry of the system. A good example is surface waves on a water layer. Here, the behavior of the solutions in the vertical direction (z) is very different from those in the horizontal ones. For shallow water waves (wave length long compared to the layer depth) the velocities are more or less independent on z, where in the other limit of deep water waves, fluid motion takes only place along a small layer under the surface and decreases exponentially with depth. In both cases one may reduce the dimension of the basic problem by an expansion with respect to simple functions for the vertical dependence of the variables (Cohen and Kundu 2004). An analogue method can be applied describing thin film surface patterns (Oron et al. 1997). Also for convection cells, the vertical dimension plays a special role and the solution

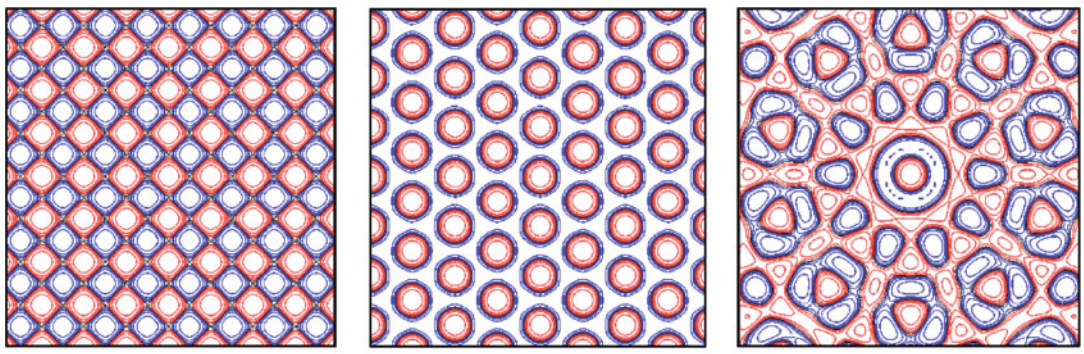

Fluid Dynamics, Pattern Formation, Fig. 2 The composition of plane waves with the same wave number but different orientation in 2D space results in regular patterns. For two modes ($N = 2$) one sees squares, for $N = 3$ hexagons and for $N > 3$ quasi periodic structures in space or Penrose tilings (Penrose 1974) are found

can be projected onto a few modes near the critical point (Busse 1967; Pesch 1996).

Another concept that reduces the number of dependent variables and equations is that of order parameters. The notion of the "order parameter" goes back to Landau (Landau and Lifshitz 1996) and refers originally to a variable that measures the order of a certain system. Rather a variable than a parameter, the order parameter normally depends on time and, in theories describing the formation of natural patterns, also on space (Newell and Whitehead 1969). Thus, the order parameter equation (abbreviated: OPE) is a partial differential equation with certain nonlinear terms that become important for pattern selection and saturation.

Theoretical methods developed by the Haken school (Haken 1983, 1975, 2004) starting in the 1970s allow for a systematic derivation of the OPEs (sometimes also called "generalized Ginzburg–Landau equations") for a great variety of nonequilibrium and open systems from physics, chemistry and biology. The key idea is to find a reduced description in terms of relevant or active modes close to a certain bifurcation point. The amplitudes of these active modes, the order parameters, now generalized to a nonequilibrium, pattern forming system, obey unified and simplified equations, namely the OPEs. It turns out that the structure of these equations depends not so much on the particular system under consideration as on the type of bifurcation. To each type of bifurcation a special "normal form" of OPE is related (Cross 1988). In deriving the OPEs, the slaving principle (Haken 2004) allows us to eliminate a huge number of slaved variables and express them by the active ones.

This contribution is concerned mainly with structures in fluids that originate from self-organized processes. It tries to bring together direct numerical solutions of hydrodynamic equations with the modern concepts of pattern formation. After introducing the basic equations (Section "The Basic Equations of Fluid Dynamics") of fluid dynamics, it presents a short section on waves and descriptions reduced by geometrical reasons. Several types of instabilities are discussed in Section "Instabilities", together with computer solutions for the different cases. Section "Order Parameter Equations" presents different types of two-dimensional order parameter equations. Finally, Section "Conserved Order Parameter Fields" is devoted to the special case of conserved order parameters.

The Basic Equations of Fluid Dynamics

Let the state of a fluid be described by its velocity, its density, its pressure, and its temperature field

$$\vec{v}\left(\vec{r},t\right),\ \rho\left(\vec{r},t\right),\ p\left(\vec{r},t\right),\ T\left(\vec{r},t\right). \qquad (1)$$

In this section we wish to specify the basic hydrodynamic equations that rule the spatio-temporal behavior of these seven variables. They have to be completed by suitable boundary conditions (abbreviated: b.c.) which we shall present later with the particular systems under consideration.

Continuity Equation

The conservation of mass yields the continuity equation

$$\partial_t \rho + \mathrm{div}\left(\rho\vec{v}\right) = \partial_t \rho + \left(\vec{v}\cdot\nabla\right)\rho + \rho\ \mathrm{div}\ \vec{v} = 0. \qquad (2)$$

In most cases, liquids are difficult to compress. One can usually assume that a volume element does not change its density while it moves with the fluid (Lagrangian description)

$$\partial_t \rho + \left(\vec{v}\cdot\nabla\right)\rho = 0.$$

From (2) one finds the condition of incompressibility

$$\mathrm{div}\ \vec{v}\left(\vec{r},t\right) = 0, \qquad (3)$$

or, in other words, the velocity field is free of sources and sinks. Equation (3) can be satisfied by the ansatz

$$\vec{v}\left(\vec{r},t\right) = \mathrm{curl}\,\vec{A}\left(\vec{r},t\right) \tag{4}$$

where $\vec{A}$ plays the role of a vector potential. In (4) one can use the particular decomposition (Bestehorn 1993; Chandrasekhar 1961)

$$\begin{aligned}\vec{v}\left(\vec{r},t\right) &= \mathrm{curl}(\Phi\hat{\mathrm{e}}_z) + \mathrm{curl}\,\mathrm{curl}(\Psi\hat{\mathrm{e}}_z)\\ &= \begin{pmatrix}\partial_y\Phi + \partial_z\partial_x\Psi\\ -\partial_x\Phi + \partial_z\partial_x\Psi\\ -\Delta_2\Psi\end{pmatrix}\end{aligned} \tag{5}$$

with the two independent scalar functions $\Phi\left(\vec{r},t\right)$ and $\Psi\left(\vec{r},t\right)$ and $\Delta_2 = \partial_{xx}^2 + \partial_{yy}^2$ as the 2D-Laplacian.

If the velocity field is irrotational, that is without vortices $\left(\mathrm{curl}\,\vec{v} = 0\right)$, it can be derived from a scalar potential

$$\vec{v} = \mathrm{grad}\,\phi. \tag{6}$$

For incompressible and irrotational flows, hydrodynamics is reduced to a boundary value problem, since the potential must fulfill the Laplace equation

$$\mathrm{div}\,\vec{v} = \Delta\phi = 0 \tag{7}$$

and the velocity field is solely determined by its boundary conditions.

Euler Equations

For a perfect fluid, a fluid with no viscosity, one derives the Euler equations from the law of conservation of momentum (Lai et al. 1993). They read

$$\begin{aligned}&\rho\left(\vec{r},t\right)\left[\partial_t\vec{v}\left(\vec{r},t\right) + \left(\vec{v}(\vec{r},t)\cdot\nabla\right)\vec{v}(\vec{r},t)\right] =\\ &-\mathrm{grad}\,p\left(\vec{r},t\right) + \vec{f}\left(\vec{r},t\right),\end{aligned} \tag{8}$$

where $\vec{f}$ denotes external volume forces. Together with a state equation of the form

$$p = p(\rho,T), \tag{9}$$

the continuity Eq. (2) and the temperature equations (to be shown below) (Subsection "Transport Equations") constitute the basic set for the seven state variables (1).

Incompressible Fluids For an incompressible fluid, a state equation of the form (9) makes no sense since pressure will not change with density. So p can be eliminated by forming the curl of (8)

$$\partial_t\vec{\Omega} = \mathrm{curl}\left(\vec{v}\times\vec{\Omega}\right) + \frac{1}{\rho}\mathrm{curl}\,\vec{f} \tag{10}$$

Where

$$\vec{\Omega} = \mathrm{curl}\,\vec{v} \tag{11}$$

denotes the vorticity. If p must be known, it can be computed from the divergence of (8) which yields

$$\nabla^2 p = \rho\left\{-\mathrm{Tr}\left[\left(\nabla\circ\vec{v}\right)\left(\nabla\circ\vec{v}\right)\right] + \mathrm{div}\,\vec{f}\right\}, \tag{12}$$

where $\circ$ is the dyadic product and Tr[. . .] the trace.

Incompressible Irrotational Fluids If, in addition, the flow is free of vortices, one may integrate the Euler equations and find the theorem of Bernoulli

$$\partial_t\phi = -\frac{1}{\rho}(p+U) - \frac{1}{2}(\nabla\phi)^2 \tag{13}$$

where U is the potential to $\vec{f}$ ($\vec{f}$ must be irrotational, too). For stationary solutions, the velocity potential ϕ is found from (7) and (13) can be used to determine the pressure.

Navier–Stokes Equations

Compressible Fluids In real fluids, shear stresses are a result of friction. They must be added to the balance of momentum and yield the Navier–Stokes equations. For a compressible Newtonian fluid they read

$$\begin{aligned}&\rho\left[\partial_t\vec{v} + \left(\vec{v}\cdot\nabla\right)\vec{v}\right]\\ &= -\mathrm{grad}\;\; p + \vec{f} + \eta\Delta\vec{v} + \left(\zeta + \frac{\eta}{3}\right)\mathrm{grad}\,\mathrm{div}\,\vec{v}\end{aligned} \tag{14}$$

where η denotes the first and ζ the second viscosity (Landau and Lifshitz 2004).

Incompressible Fluids The Navier–Stokes equations for incompressible fluids are simpler:

$$\rho\left[\partial_t \vec{v} + \left(\vec{v}\cdot\nabla\right)\vec{v}\right] = -\nabla p + \vec{f} + \eta\Delta\vec{v}. \tag{15}$$

Again, pressure can be eliminated by forming the curl. Taking the ansatz (5), the z-components of the curl and of the curl of the curl of (15), we have

$$\{\nu\Delta - \partial_t\}\,\Delta_2\Phi\left(\vec{r},t\right) = \left[\mathrm{curl}\left(\left(\vec{v}\cdot\nabla\right)\vec{v}\right)\right]_z + \frac{1}{\rho}\left(\partial_x f_y - \partial_y f_x\right) \tag{16a}$$

$$\{\nu\Delta - \partial_t\}\,\Delta\Delta_2\Psi\left(\vec{r},t\right) = \left[\mathrm{curl}\,\mathrm{curl}\left(\left(\vec{v}\cdot\nabla\right)\vec{v}\right)\right]_z + \frac{1}{\rho}\left(\Delta_2 f_z - \partial_x\partial_z f_x - \partial_y\partial_z f_y\right). \tag{16b}$$

Here we have introduced the kinematic viscosity $\nu = \eta/\rho$. We note that this decomposition is of particular interest if $f_x = f_y = 0$ as is the case in convection problems of a plane layer.

Incompressible Fluids with a Small Reynolds Number

For some applications it is convenient to use the Navier–Stokes equations in dimensionless form. With scaling with respect to a characteristic length L and velocity V_0:

$$\vec{r} = L\cdot\vec{r}', t = (L/V_0)\cdot t', \vec{v} = V_0\cdot\vec{v}', p' = \frac{L}{\eta V_0}\cdot p,$$

(15) turns into

$$R_e\left[\partial_t\vec{v}' + \left(\vec{v}'\cdot\nabla'\right)\vec{v}'\right] = -\nabla' p' + \Delta'\vec{v}'. \tag{17}$$

(We assumed a potential for $\vec{f}$ which can be confined into p.) The dimensionless quantity

$$R_e = \frac{LV_0}{\nu} \tag{18}$$

is the Reynolds number. If $R_e \ll 1$, the left hand side of (17) can be neglected and the Navier–Stokes equations become linear (primes omitted):

$$\Delta\vec{v} = \nabla p. \tag{19}$$

This is the Stokes equation, in which no time derivative of $\vec{v}$ occurs. Thus, as known from over-damped motion, the velocity field directly follows the pressure gradients.

Transport Equations

Scalar fields such as temperature or concentration of a mixture that may diffuse into and be transported with the fluid are ruled by the transport equation. Let $S\left(\vec{r},t\right)$ be the scalar field, then the transport equation reads

$$\partial_t S + \left(\vec{v}\cdot\nabla\right)S = D_s\Delta S, \tag{20}$$

where D_s is the appropriate diffusion coefficient.

Surface Waves

The only elastic forces in fluids are those coming from volume changes and may exist, therefore, only in compressible fluids. They give rise to longitudinal compression waves which usually have small amplitudes and behave linearly in a good approximation. A linear wave equation can be derived with a (space dependent) sound speed (Lai et al. 1993).

A transversal wave which is also possible in incompressible fluids can be formed along a deformable interface. Gravity and, for small wavelengths, surface tension provide the stabilizing mechanism of a flat surface, around which oscillations (gravity waves) may occur. If their amplitudes are big enough, nonlinearities may play an essential role for surface waves, as is clearly seen by solitons (Drazin et al. 1989; Nekorkin and Velarde 2002) and wave breaking (Dean and Dalrymple 2000). For this reason we shall discuss only surface waves in this section.

Gravity Waves

If one assumes an irrotational flow of a perfect and incompressible fluid on a flat substrate and with a free, deformable surface (Fig. 3), then the velocity

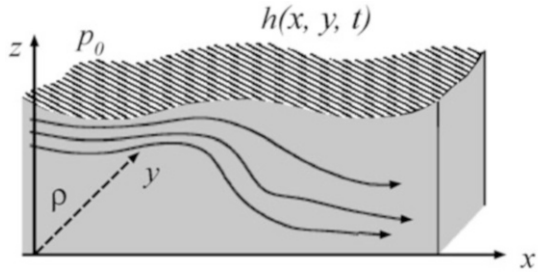

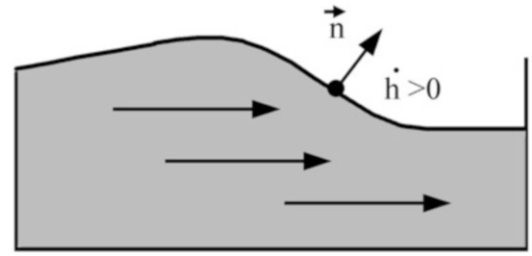

Fluid Dynamics, Pattern Formation, Fig. 3 *Left:* an (incompressible) fluid with a free and deformable surface located at $z = h(x, y, t)$, on which a constant external pressure p_0 is applied. *Right:* The location of a certain point of the surface changes if the fluid is in motion

is determined by the Laplace Eq. (7) which must be accomplished by boundary conditions at $z = 0$

$$v_z|_{z=0} = \partial_z \phi|_{z=0} = 0 \tag{21}$$

and at $z = h(x, y, t)$

$$\partial_t \phi\Big|_{z=h} = -gh - p(h)/\rho - \frac{1}{\rho}(\nabla\phi)^2 \tag{22}$$

where g denotes the gravitational acceleration. Equation (22) is nothing other than the Bernoulli Eq. (13) evaluated at the surface. The surface itself is determined by the so-called kinematic boundary condition that reads (see Fig. 3, right frame).

$$\begin{aligned}\partial_t h &= v_z\big|_{z=h} - v_x\big|_{z=h}\partial_x h - v_y\big|_{z=h}\partial_y h \\ &= \partial_z\phi\big|_{z=h} - (\partial_x h)(\partial_x\phi)_{z=h} - \big(\partial_y h\big)\big(\partial_y\phi\big)_{z=h}.\end{aligned} \tag{23}$$

Shallow Water Equations

For shallow water waves, one can introduce the small parameter

$$\delta = \mathrm{d}/l \tag{24}$$

which is the ratio of the water depth d and a typical horizontal scale (such as a wavelength) l. Then (7) can be solved iteratively; the result is a power series in δ^2 (Cohen and Kundu 2004; Dean and Dalrymple 2000):

$$\begin{aligned}&\phi\left(\vec{r}, t\right) = \Phi(x, y, t) \\ &+\delta^2\left[-\frac{z^2}{2}\Delta_2\Phi(x, y, t) + \varphi^{(1)}(x, y, t)\right] + O\left(\delta^4\right)\end{aligned} \tag{25}$$

with an arbitrary function φ_1. Inserting (25) into (23) and (22) yields up to the lowest order in δ the *shallow water equations*

$$\begin{aligned}\partial_t h = &-h\Delta_2\Phi - (\partial_x h)(\partial_x\Phi) \\ &- \big(\partial_y h\big)\big(\partial_y\Phi\big)\end{aligned} \tag{26a}$$

$$\begin{aligned}\partial_t\Phi = &-gh - p(h)/\rho - \frac{1}{2}(\partial_x\Phi)^2 \\ &- \frac{1}{2}\big(\partial_y\Phi\big)^2.\end{aligned} \tag{26b}$$

This is the first example of how to derive a two-dimensional system starting from three-dimensional fluid motion. Eq. (26) constitute a closed system of partial differential equations for the evolution of the two functions $h(x, y, t)$ and $\Phi(x, y, t)$. Using (25), one immediately finds from the latter the velocity field (up to the order δ^2).

Numerical Solutions

Figure 4 shows numerical solutions of the shallow water equations (left frame in one dimension, right frame in two dimensions). In one dimension, one sees clearly traveling surface waves which may run around due to the periodic boundary conditions in x. On the other hand, one can recognize a second wave with a smaller amplitude going to the left hand side. Both waves seem to penetrate each other without further interaction. The reason seems to be the smallness of the amplitude which results in a more or less linear behavior. In the two-dimensional frame, a snapshot of the temporal evolution of the surface is presented. The initial condition was chosen randomly. For numerical stability reasons, an additional damping of the form $\tilde{\nu}\Delta_2\Phi$ was added to the right hand side of (26b) which filters out the short wave lengths. This could be justified phenomenologically by friction and leads in the long term to a fluid at rest, if only gravity acts.

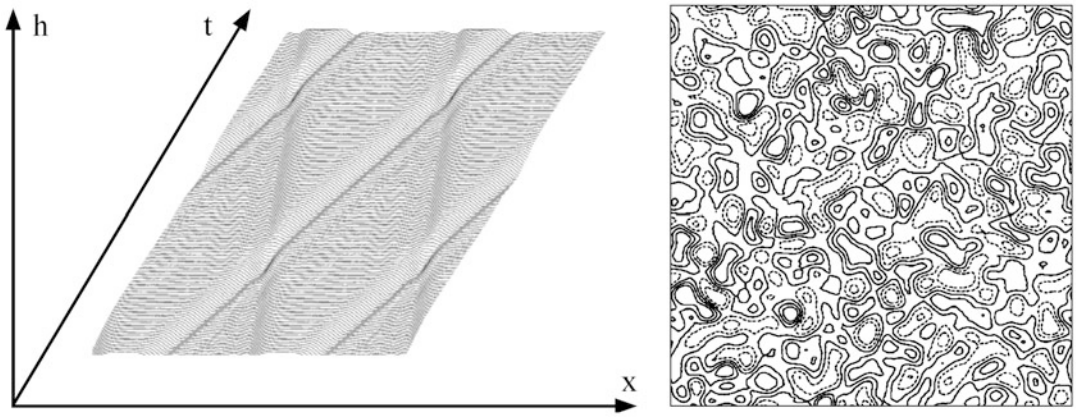

Fluid Dynamics, Pattern Formation, Fig. 4 Numerical solutions of the shallow water equations, *left frame* shows a temporal evolution in one dimension, *right frame* a snapshot in two dimensions. *Dashed contour lines* mark troughs, *solid ones* correspond to peaks of the sea

Instabilities

Laplace Pressure and Disjoining Pressure To discuss Eq. (26) further, we must elaborate a little on the dependence of the surface pressure on the depth $h(x, y, t)$ and on its curvature $-\Delta h$.

The length scale of the surface structures is proportional to the depth of the fluid layer. If the films are very thin, we expect to have scales in the range or even well below the capillary length $a = \sqrt{\Gamma/g\rho}$ where Γ denotes the surface tension. Then one has to take into account the additional pressure which originates from the curvature of the surface, the so-called *Laplace pressure* (Landau and Lifshitz 2004) $-\Gamma\Delta_2 h$. Thus we substitute in (26b)

$$p(h) = p_1(h) - \Gamma\Delta_2 h, \tag{27}$$

with a function p_1 (the disjoining pressure) that will be specified later (de Gennes 1985; Van Oss et al. 1988).

Linear Stability Analysis of the Flat Surface To see if the flat film $h = h_0$ is stable against small perturbations, one may perform a linear stability analysis. Inserting

$$(h - h_0, \Phi) = (a, b) \exp\,(\lambda t + ikx)$$

into (26) yields, after linearization with respect to a, b, a linear eigenvalue problem with the solvability condition

$$\begin{aligned}\lambda_{12}(k) &= -\frac{\tilde{\nu}k^2}{2} \\ &\pm i\,|k|\,\sqrt{h_0\left(g + p_1' + \Gamma k^2\right)/\rho - \tilde{\nu}^2 k^2/4},\end{aligned} \tag{28}$$

where

$$p_1' = \left.\frac{\mathrm{d}p_1}{\mathrm{d}h}\right|_{h=h_0}.$$

We assume that the artificial viscosity is small, $\tilde{\nu}^2 \ll \Gamma/\rho$. An instability occurs first at $k = 0$ if the expression under the integral can be negative, that is, for $p_1' + \rho g < 0$. This corresponds to the region of initial thickness h_0 where the generalized pressure

$$p_1(h) + \rho g h \tag{29}$$

has a negative slope. For that case, the real part of λ_1 starts at $k = 0$ at zero with positive slope, has a maximum at $k = k_c$ and decreases again to the value $-\nu k^2/2$. We shall revisit this instability in the next section and call it there, in a more systematic classification, a type II instability. How can (29) have a negative slope for a certain range of h_0? It is obvious that one has to assume that the pressure p_1 depends in some nonlinear nonmonotonic fashion on the value of h (Fig. 5). As we shall see later, this can be the case for very thin films where van der Waals forces between the solid support and the

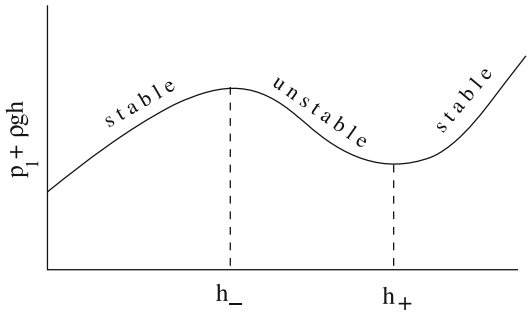

Fluid Dynamics, Pattern Formation, Fig. 5 If the pressure depends on h and has a certain region with a negative slope, the flat film is unstable in this region and pattern formation sets in

free surface come into play (de Gennes 1985; Israelachvili 1992; Van Oss et al. 1988). But also, in thicker films, this should be possible in non-isothermal situations, where the surface temperature, and therefore the surface tension, changes with the vertical coordinate (Marangoni effect, see Section "Instabilities", Fig. 8). If we take (for instance) as a model the polynomial

$$p_1 = c \cdot h \cdot (h - h_1) \cdot (h - h_2), c > 0, \qquad (30)$$

then the flat surface is unstable for h between the two spinodals

$$h_- < h < h_+$$

with $h_\pm$ being the roots of

$$3h^2 - 2h(h_1 + h_2) + h_1 h_2 + \rho g/c = 0.$$

Figure 6 shows a numerically determined time series of a random dot initial condition. The mean thickness h_0 was chosen in the unstable region. The formation shows traveling waves in the linear phase, followed by coarsening to a large scale structure, in this case one big region of depression, or a hole. This hole becomes more and more symmetric while the velocity decays due to the friction term. Finally, a steady state of a big circular hole remains.

Parametric Excitation of a Thin Bistable Fluid Layer

One way to replace the energy lost by damping (to "open" the system) is to accelerate the whole layer periodically in the vertical direction. This was done first in an experiment by Michael Faraday in 1831 (Faraday 1831). He obtained regular surface patterns normally in the form of squares, see Fig. 1.

Faraday patterns can be seen as a solution of the shallow water equations if the gravity constant g is modulated harmonically (Bestehorn 2006)

$$g(t) = g_0 + g_1 \cos \omega t. \qquad (31)$$

A linear stability analysis leads to a Mathieu Eq. (1). The flat film is unstable if frequency and amplitude fall into certain domains, the so-called *Arnold tongues*. There, one usually finds squares for not-too-supercritical values.

We conclude this section by showing a numerical solution of (26) with parameters as in Fig. 6, but now with an additional periodic excitation (Fig. 7). Coarsening is still present, but now oscillating drops emerge in the form of stars. No time stable structure is found in the long time limit.

Instabilities

Mechanisms of Instability in Fluids

We start with the specific case of a plane layer of a viscous fluid with a vertically applied, constant temperature gradient β (Fig. 11), where

$$\beta = (T_1 - T_0)/d \qquad (32)$$

and T_0, T_1 are the temperatures at the lower, upper side of the layer. We assume that a motionless stationary state exists as a (stable or unstable) solution of (15) and of an equation such as (20) for the temperature. The temperature and pressure distribution of that state can then be computed from (15, 20) by putting $\vec{v}$ and all time derivatives to zero:

$$\nabla p^0 = \vec{f} \qquad (33a)$$

$$\Delta T^0 = 0. \qquad (33b)$$

If an external force is provided by buoyancy, we may align the z-axis of the coordinate system along $\vec{f}$ which yields

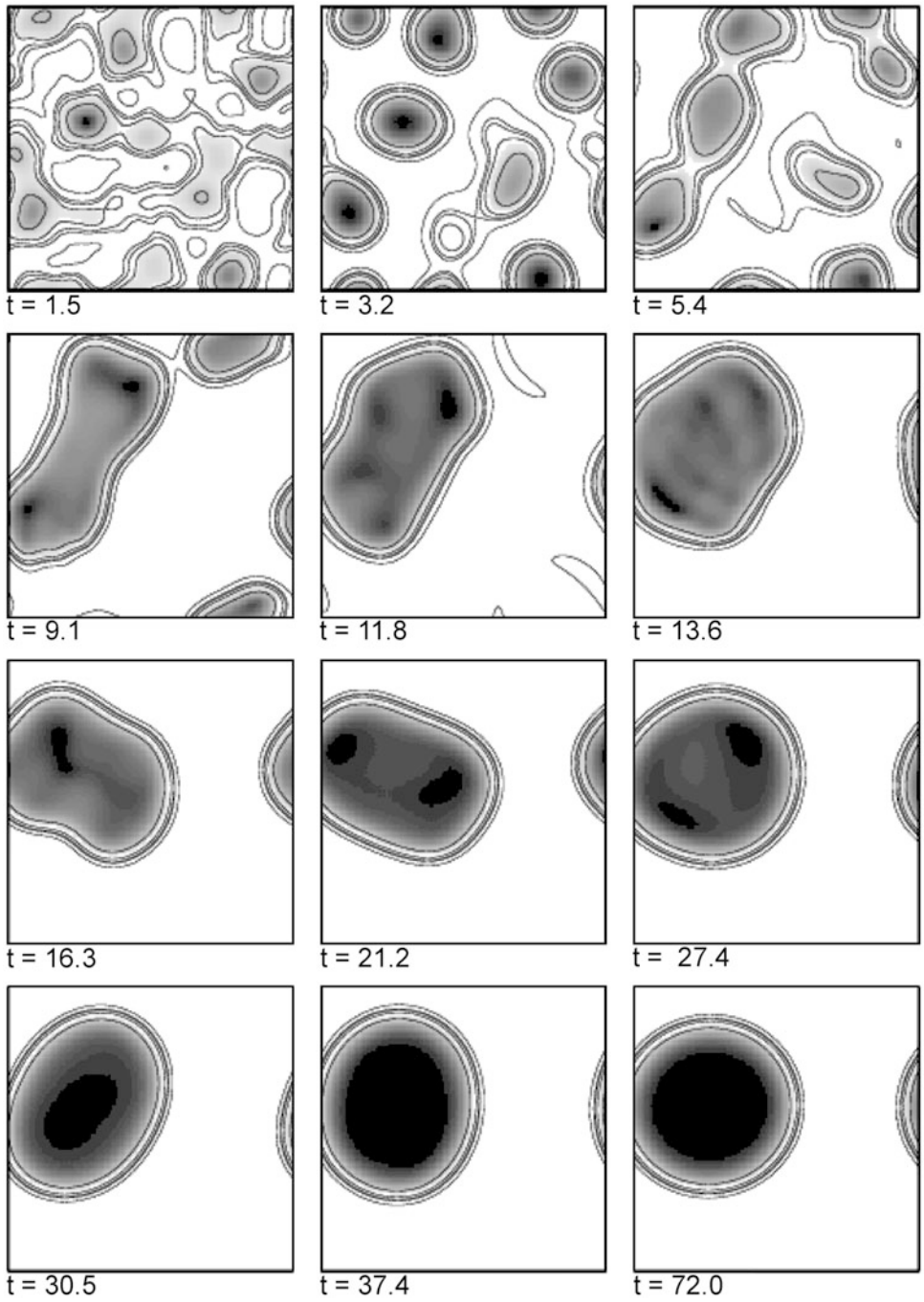

Fluid Dynamics, Pattern Formation, Fig. 6 Time series from a numerical solution of (26) with artificial damping and bistable pressure according to (30). Coarsening dominates the nonlinear evolution and eventually a stationary circular region of surface depression (a hole) remains. Periodic boundary conditions in both horizontal directions have been used

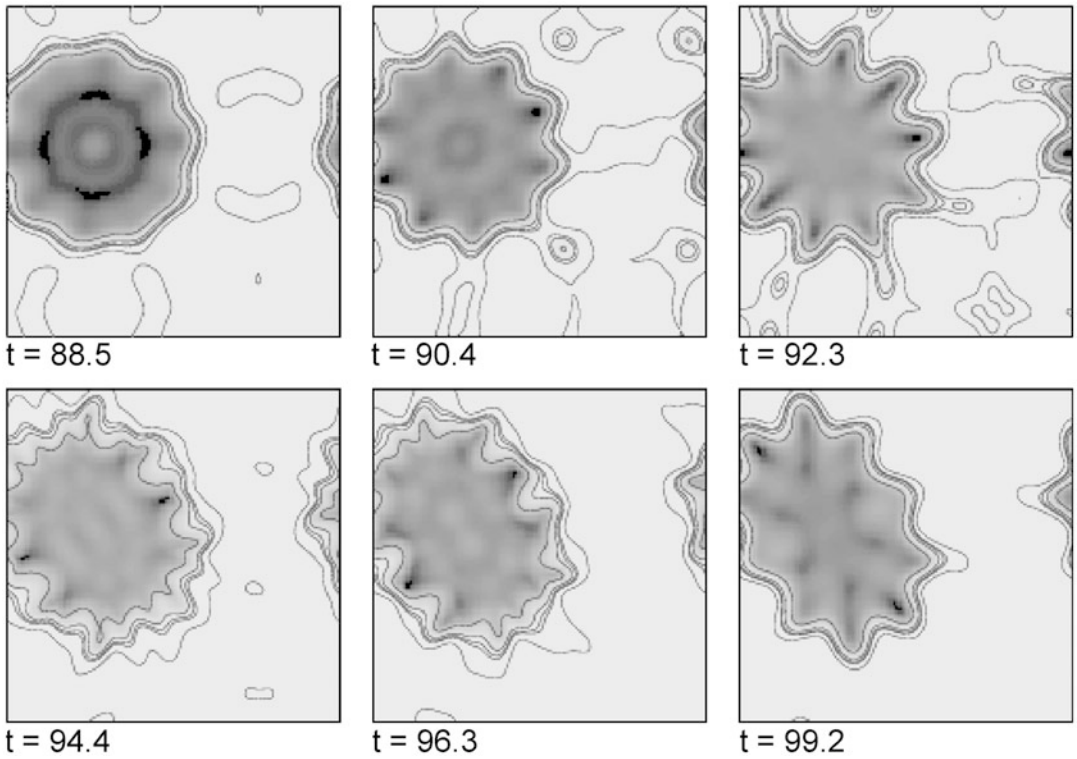

Fluid Dynamics, Pattern Formation, Fig. 7 Continuation of the series of Fig. 6, but with additional parametric excitation according to (30) switched on at $t = 72$. Instead of stationary patterns pulsating stars are found

$$\vec{f} = -g\,\rho\left(\vec{r}\right)\,\hat{\mathrm{e}}_z,$$

where g is the gravitational acceleration. Equation (33a) can be solved only if ρ does not depend on x and y. If one assumes that the density depends on temperature

$$\rho = \rho\left(T^0\right) \tag{34}$$

then T^0 can also depend only on z. Thus one finds from (33b)

$$T^0(z) = a + bz. \tag{35}$$

Taking a linear relation for (34)

$$\rho(T) = \rho_0[1 - \alpha(T - T_0)] \tag{36}$$

with the heat expansion coefficient $\alpha \equiv -\rho_0^{-1}\mathrm{d}\rho/\mathrm{d}T$ and ρ_0 as the density at the reference temperature T_0, one may integrate (33a) and find for the pressure of the motionless state (hydrostatic pressure)

$$p^0(z) = -g\int \rho \mathrm{d}z = -g\rho_0\left(z - \frac{1}{2}\alpha\beta z^2\right) \tag{37}$$

where we put $a = T_0$ and $b = \beta$, in agreement with (32).

A linear stability analysis (Chandrasekhar 1961) shows that the motionless, nonequilibrium state (35) can become unstable if the temperature gradient β exceeds a certain critical value, depending on the fluid properties and the geometry of the layer. There are two different mechanisms, if the fluid layer is heated from below:

(1) *Buoyancy:* Hot fluid particles (volume elements) near the bottom are lighter than colder ones and want to rise. Colder particles near the top want to sink. If the stabilizing forces of

thermal conduction and friction in the fluid are exceeded by the externally applied temperature gradient, patterned fluid motion sets in.

(2) *Surface tension:* If the upper surface of the fluid is free, that is, in contact with the ambient air, tangential surface tension normally increases with decreasing surface temperature (Fig. 8a–c). If a fluid particle near the surface moves by fluctuations, say, to the right, then warmer fluid is pulled up from the bottom, increasing the surface temperature locally. Due to laterally increasing surface tension with respect to the neighbored points, even more hot fluid is pumped up from the bottom and the fluid starts to move. This is called the Marangoni effect and works even without gravity, that is, in space experiments.

In both cases, the typical length of the structures which bifurcate from the motionless state is of the order of the layer depth. These instabilities are sometimes called *small scale instabilities.*

In the situation described above, the surface can be assumed to be flat and undeformable. Of course this is only an approximation, but valid for not-too-thin fluid layers and parameters not too far from threshold. If, on the other hand, the thickness of the fluid layer is less than a certain value which is on the order of 10^{-4} m for common silicone oils, another mechanism comes to the foreground. This mechanism is based on

Surface Deformation. If the surface is locally depressed by an arbitrary fluctuation, the depressed part is heated up due to the vertical temperature gradient. A lateral surface tension gradient is formed which pulls the liquid outside the depressed region (Fig. 8d). Since the continuity equation must hold, the surface becomes even more depressed and an instability occurs. The same mechanism leads to the growth of elevated parts of the surface, under which fluid is pumped in from adjacent regions (Golovin et al. 1997; Nepomnyashchy et al. 2002; Oron et al. 1997). The deformation mode belongs to the so-called *large-scale instability.* This means that the fastest growing modes have a wavelength that is very large compared to the layer depth. It is the depth of the layer which distinguishes which instability occurs first if the temperature gradient is increased from the sub-critical region (Fig. 9).

In ultra-thin films (depth of few 100 nm or less), other mechanisms are possible. Van der Waals forces between the free surface and the solid substrate then become important. They have a potential and can be expressed in the pressure by an extra term, *disjoining pressure,* as already shown in Section "Surface Waves". If that pressure increases with decreasing layer depth, fluid is pressed out of depressed regions and pumped into elevated regions and an instability occurs, even for isothermal cases (Fig. 10).

Pattern Formation – Examples

What happens if the critical value for the temperature gradient is exceeded? Since the famous experiments of Henri Bénard (Bénard 1901) in the beginning of the twentieth century, one knows that the fluid starts to move in form of hexagons if the surface is free and the layer is "thick" (Fig. 11). These kinds of experiments

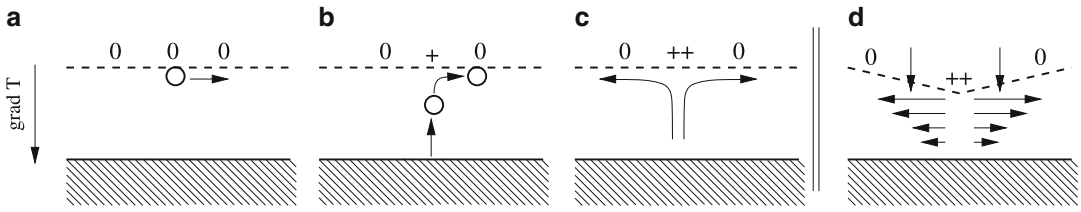

Fluid Dynamics, Pattern Formation, Fig. 8 **a-c** The Marangoni effect may destabilize a fluid layer at rest and may generate a (regular) fluid motion. The surface remains flat (to a good approximation). If the surface is deformable d, a large scale instability may occur as a consequence of the Marangoni effect and mass conservation. For both instabilities, it is sufficient to assume the surface tension as a linear function of temperature. (+/-/0) denote relative temperatures

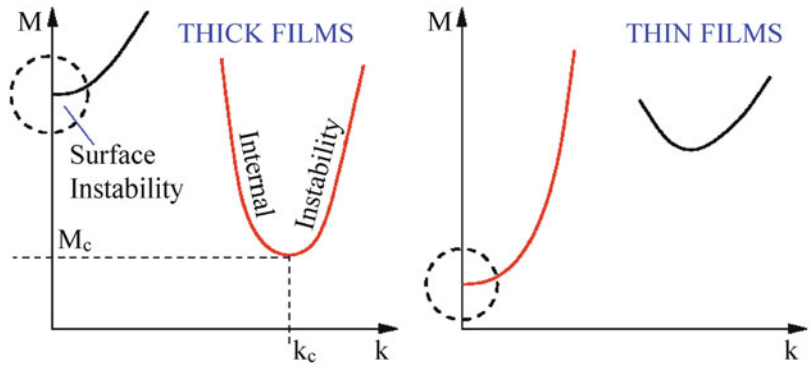

Fluid Dynamics, Pattern Formation, Fig. 9 The two cases "thick films" and "thin films" are defined by the instability that comes first when the temperature gradient is increased. The two instabilities differ in the wavelength Λ (wave number $k = 2\pi/\Lambda$) of the growing structures

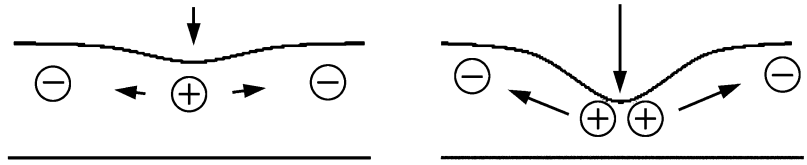

Fluid Dynamics, Pattern Formation, Fig. 10 In ultra-thin films (Reiter et al. 1999; Sharma and Khanna 1999; Vrij 1966), van der Waals forces between free surface and solid substrate may destabilize a plane fluid layer even without an external temperature gradient (+/− denote relative values of the disjoining pressure)

were repeated many times under excellent conditions, for free and closed surfaces, with different fluids, even under micro gravity conditions (Koschmieder 1993; Schwabe 2006).

Surprisingly, a secondary instability takes place for a larger external temperature gradient, which was not known before 1995, almost 100 years after Bénard. This instability shows the occurrence of rather regular squares and was discovered by Eckert and Thess in Dresden, Germany (Bestehorn 1996; Eckert et al. 1998; Nitschke-Eckert and Thess 1995) and, in the meantime but independently, by Schatz and Swinney in Austin, Texas (Schatz and Neitzel 2001; Schatz et al. 1999) (Fig. 12).

If the fluid is covered by a good thermal conductor (a sapphire plate, for instance), hexagons are not the typically found structure at onset, but rather stripes or rolls are encountered (Van Dyke 1982). This can be understood in the frame of reduced order parameter equations by simple symmetry arguments. We shall discuss this in more detail in Section "Order Parameter Equations". For small Prandtl numbers (the ratio between viscosity and thermal diffusivity of the fluid) more complicated

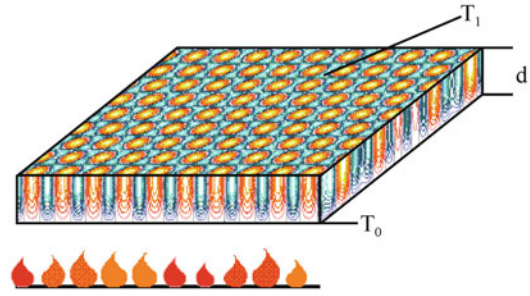

Fluid Dynamics, Pattern Formation, Fig. 11 Hexagonal motion of a fluid heated from below, found by computer solution. Shown are contour lines of the temperature field (after Bestehorn 1993)

and time dependent patterns are found in the form of spirals (Fig. 13) (Bestehorn et al. 1994; Morris et al. 1993; Pesch 1996).

The initial growth of patterns, with a certain horizontal length scale of the order of the depth of the fluid layer, is typical for pattern formation in thick films. In the long term, these structures can be stationary or time dependent, depending on several control and fluid parameters (temperature gradient, material properties, etc.). On the other

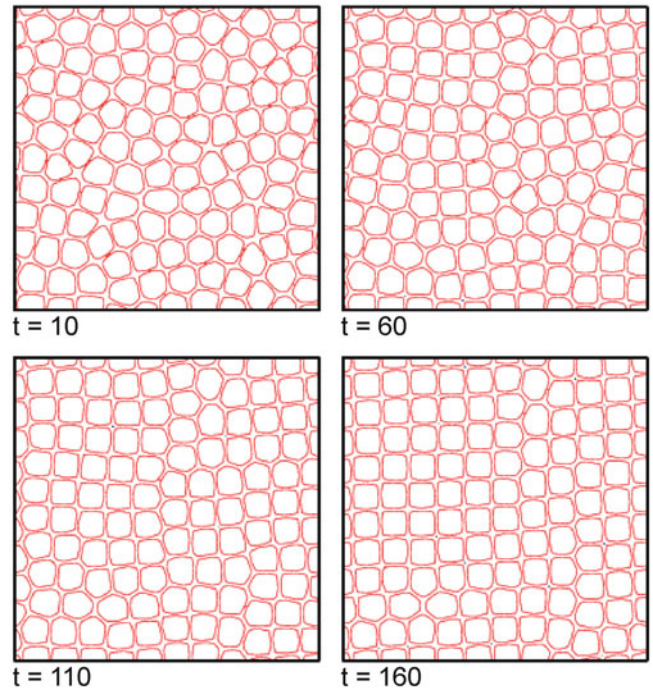

Fluid Dynamics, Pattern Formation, Fig. 12 Regular squares as a secondary instability of hexagons. Numerical solution of the basic Eq. (6)

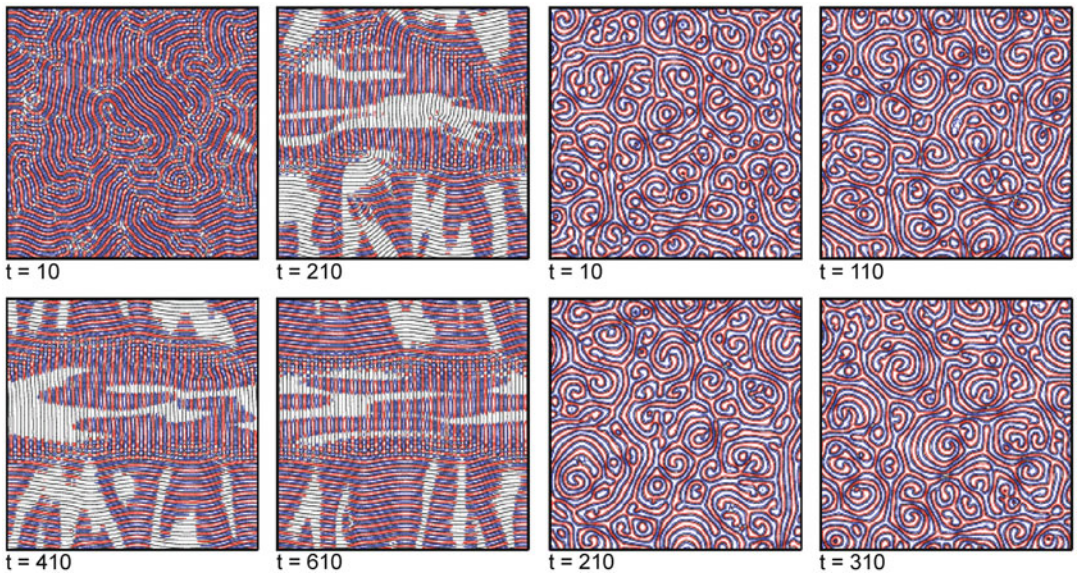

Fluid Dynamics, Pattern Formation, Fig. 13 *Left:* Rolls for high Prandtl number (Pr) fluids; *Right:* spirals for low Pr are found if the surface is covered by a good thermal conductor

hand, the spatio-temporal behavior is completely different for thin and ultra-thin films. Here one finds, after a rather short initial phase, the formation of larger and larger structures, known as *coarsening*. Eventually, the dynamics converge to a stationary state that consists of a single elevation (drop) or suppression (hole) on the surface (Fig. 14 left panel). This development can be interrupted by rupture of the film. Rupture is obtained if the surface touches the substrate and

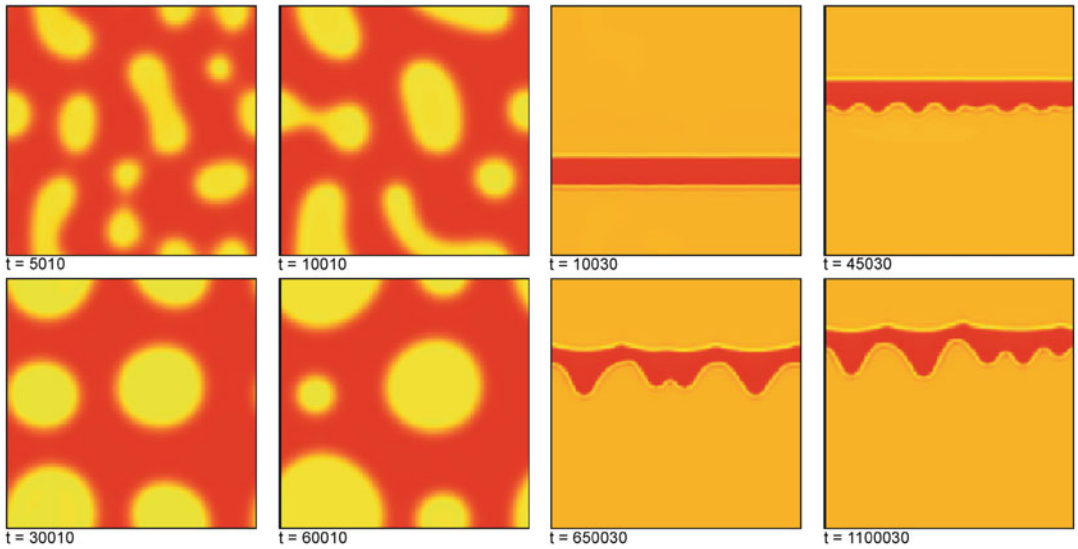

Fluid Dynamics, Pattern Formation, Fig. 14 Numerical solution of the thin film equation (see Section "Conserved Order Parameter Fields"), *red:* elevation, yellow: suppression. *Left:* Coarsening is the typical spatial behavior for a thin film. Finally, a stationary solution consisting of one single hole would survive. *Right:* If the layer is inclined, the motion of fronts and the development of front instabilities can be examined. From (Bestehorn et al. 2003)

the thickness reaches zero in certain domains. Rupture can be avoided by introducing a repelling disjoining pressure acting for a very small depth. In this situation, a completely dry region cannot exist but the substrate is, rather, covered by a so-called (ultra thin) precursor film (de Gennes 1985; Oron et al. 1997), already proposed by Hardy in 1919 (Hardy 1919).

If, in addition, horizontal forces are applied, that is, by inclining the fluid layer, interesting studies of falling films and front instabilities can be made in the frame of the thin film equation (Bestehorn and Neuffer 2001; Scheid et al. 2002). A typical example is shown in Fig. 14, right panel.

Types of Instabilities

Different types of instabilities can be classified according to their linear behavior at onset. Consider a mode having the complex eigenvalue

$$\lambda(k^2) = i\omega(k^2) + \sigma(k^2) \qquad (38)$$

with real valued frequency ω and real valued growth rate σ. Due to rotation symmetry with respect to the horizontal coordinates, all values depend only on the modulus of the wave vector of the unstable mode (assumed as a plane wave in horizontal direction).

According to (Cross and Hohenberg 1993), we use the following notions:

Type $\mathrm{III_s}$ "s" denotes stationary or monotonic and refers to the temporal behavior of the unstable mode close to onset. The type number specifies the spatial behavior of the modes. Type III means slowly varying or even constant in space ($k \approx 0$). The spatial structure beyond instability is then mainly dominated by the geometry and boundary conditions of the system under consideration. For (38) this means

$$\omega = 0 \text{ and } \left.\frac{\mathrm{d}\sigma}{\mathrm{d}k}\right|_{k=0} = 0,$$

See Fig. 15. A typical example for a type $\mathrm{III_s}$ instability is the real Ginzbur–Landau eq. A computer solution clearly showing the spatially (and temporally) slowly varying behavior can be seen in Fig. 16.

Type $\mathrm{III_o}$ "o" stands for oscillatory and denotes a non-vanishing imaginary part of (38) at threshold. This type includes Hopf-instabilities which have the same slow spatial behavior as $\mathrm{III_s}$. In (38) we have

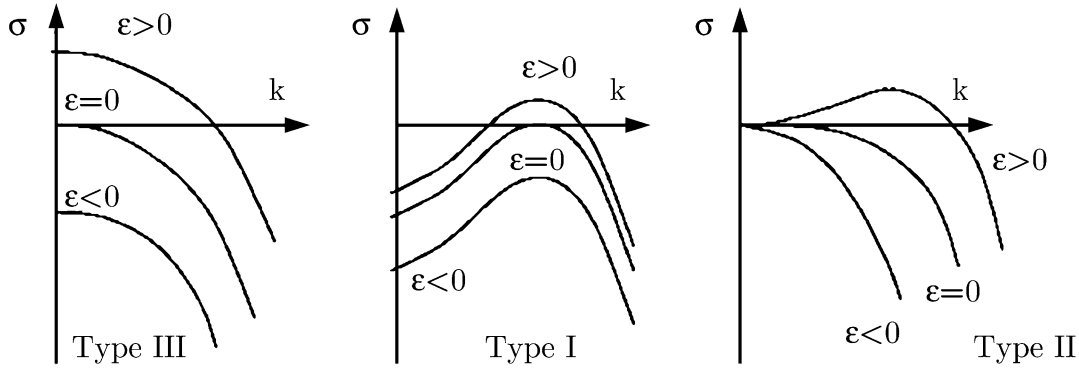

Fluid Dynamics, Pattern Formation, Fig. 15 Schematic drawing of the real part of the eigenvalue (38) as function of the wave vector for the three types of instabilities

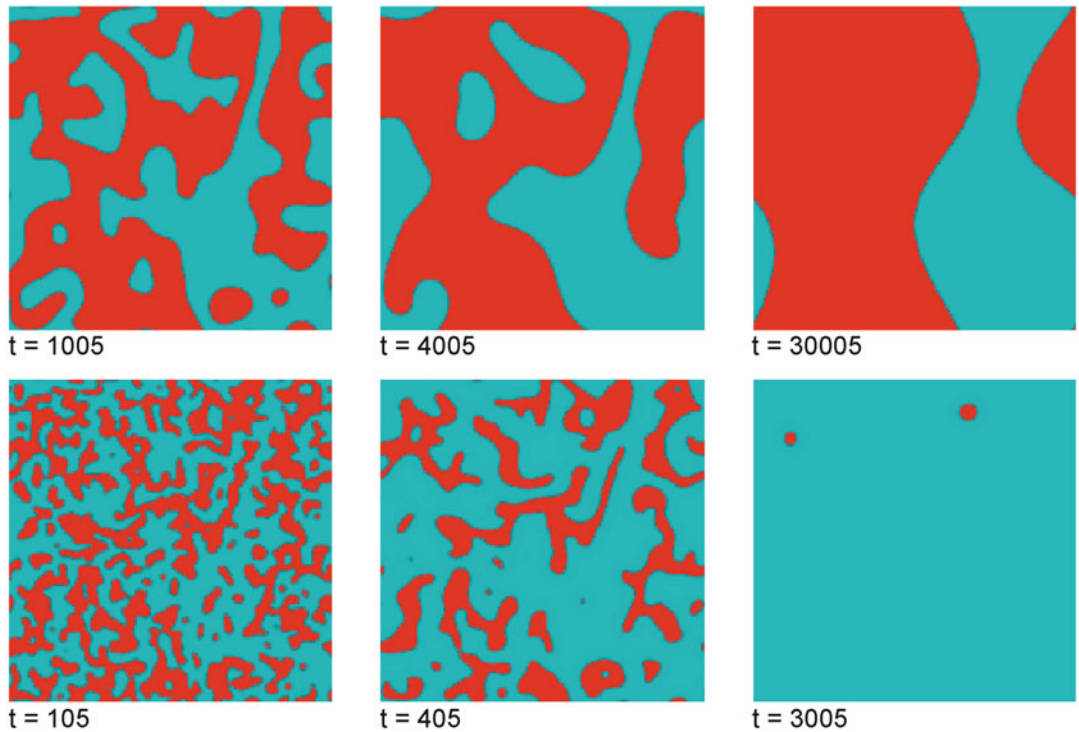

Fluid Dynamics, Pattern Formation, Fig. 16 Numerical solution (time series) of the real Ginzbur–Landau Eq. (39) which shows a III_s instability. The Ginzbur–Landau equation can be considered as a simple model for the magnetization of a ferro magnet. Then the two rows show the spatio-temporal evolution of the magnetization, *Top:* without external field, *Bottom:* with external field

$$\omega \neq 0 \text{ and } \left.\frac{\mathrm{d}\sigma}{\mathrm{d}k}\right|_{k=0} = 0.$$

For this kind of instability one needs at least two coupled diffusion equations. It is often encountered in reaction diffusion systems, as for instance the "Brusselator" (Prigogine and Levever 1968; Prigogine and Nicolis 1967).

Type I_s The short scale pattern forming instabilities shown in Figs. 11, 12 and 13 with periodicity

in space, $k_c \neq 0$ are of this type, see Fig. 15 middle frame. Again one needs at least two coupled diffusion equations to obtain such an instability. For the eigenvalue,

$$\omega = 0 \text{ and } \left.\frac{\mathrm{d}\sigma}{\mathrm{d}k}\right|_{k=k_c} = 0 \text{ with } k_c \neq 0$$

holds. Sometimes these kinds of patterns are called *Turing structures* or *Turing instabilities,* after the seminal work of Alan Turing, who predicted this patterns in skin, scales, or hair coating of certain animals (Turing 1952) (Fig. 17). For more details and pattern formation in biology see (Murray 1993).

Type $\mathbf{I_o}$ Denotes oscillating Turing structures, sometimes also called *wave instabilities.The* eigenvalue λ then has the form

$$\omega \neq 0 \text{ and } \left.\frac{\mathrm{d}\sigma}{\mathrm{d}k}\right|_{k=k_c} = 0 \text{ with } k_c \neq 0.$$

For this instability, the system must be described by at least three coupled diffusion equations. In fluid mechanics, this kind of instability can be encountered in binary mixtures and give rise to a very complicated, in general chaotic, spatio-temporal behavior just at onset (Bestehorn and Colinet 2000).

Type $\mathbf{II_s}$ This type is realized in the surface patterns of thin films, Fig. 14. Here, λ depends on k as shown in the right frame of Fig. 15. One has

$$\omega = 0 \text{ and } \left.\frac{\mathrm{d}\sigma}{\mathrm{d}k}\right|_{k=k_c} = 0 \text{ with } k_c \neq 0$$

and in addition

$$\sigma(k = 0) = 0.$$

From the last condition one sees that modes with $k = 0$, that is, those which are homogeneous in space, are marginally stable, meaning neither stable nor un stable. One may then add a constant to the order parameter (the mode amplitude)

$$\xi' = \xi + \text{const},$$

where ξ' is still a solution of the linear part of the order parameter equation. This property usually has its origin in a symmetry of the basic problem. We shall discuss this instability type in Section "Conserved Order Parameter Fields" on thin films. There, the symmetry corresponds to a global shift of the surface in vertical direction.

Type $\mathbf{II_0}$ The same as $\mathrm{II_s}$ but with an additional imaginary part $\omega \neq 0$. We mention this type only for the sake of completeness; there will be no further examples in this contribution.

Fluid Dynamics, Pattern Formation, Fig. 17 After a theory by A. Turing the painting on skin, scales, or coats of animals is organized by a nonequilibrium chemical reaction during the embryonal phase. *Left:* regular spots arranged in a hexagonal manner on the panther fish, *Right:* stripes with defects on the lion fish (pictures taken by the author in the Berlin Zoo)

Order Parameter Equations

Order Parameters

In this section, we wish to describe pattern formation in the weakly nonlinear regime. We shall mainly restrict ourselves to the case of monotonic (non-oscillatory) instabilities. For further references see (Bestehorn and Friedrich 1999; Bestehorn and Haken 1990; Cross and Hohenberg 1993; Haken 1983, 2004). Close to a bifurcation point to a new state, it is natural to expand nonlinearities with respect to small deviations from the old, unstable state. These deviations can be written as a composition of certain Galerkin functions or modes; the amplitudes of these modes are called *order parameters*. If the order parameters are functions only of time, the dynamics given by the order parameter equations (ordinary differential equations, abbreviated: ODE) are perfect patterns, for instance parallel stripes, squares (two order parameters) or hexagons (three order parameters). Natural patterns having defects and grain boundaries, as for instance the structures shown in Figs. 11, 12 and 13 can also be described in this frame. One then has to make the additional assumption that the order parameters also vary (slowly) in space and are ruled by partial differential equations (abbreviated: PDE).

The Ginzbur–Landau Eq.

A prominent (and historically the first) example of such a PDE order parameter equation is the Ginzbur–Landau equation (Aranson and Kramer 2002; Landau and Lifshitz 1996). In one spatial dimension it has the normal form

$$\partial_t \xi(x,t) = \varepsilon\,\xi(x,t) + q_0^2\,\partial_{xx}^2\,\xi(x,t) - c_3|\xi(x,t)|^2\xi(x,t) \tag{39}$$

and describes the spatio-temporal evolution of the complex order parameter field ξ. If ξ is the mode amplitude of a roll structure with a certain wave number, for example, the critical one, then stripes with defects are obtained if ξ varies (slowly) in space. If c_3 and q_0 are real valued, (39) is called the real Ginzbur–Landau equation. For complex values of the coefficients, an incomparably richer and much more complicated spatio-temporal behavior of the order parameter is encountered, for details we refer to (Aranson and Kramer 2002).

In the theory of nonequilibrium pattern formation, writing down an equation such as (39) is far from being purely phenomenological. It can be derived rather systematically from the basic hydrodynamic equations (Haken 1975; Newell and Whitehead 1969).

To give an idea of that, we do it briefly for the (two-dimensional) case of convection (the reader who is not interested in technical details can skip the rest of this section).

Starting point are the Eqs. (16) and (20) where in the latter, S stands for temperature T.

Scaling of independent $\left(\vec{r},t\right)$ and dependent $\left(\vec{v},T\right)$ variables allows the reduction of the numbers of parameters:

$$\begin{aligned}\vec{r} &= \vec{\tilde{r}}\cdot d, t = \tilde{t}\cdot\left(d^2/\kappa\right), \vec{v}\\ &= \vec{\tilde{v}}\cdot(\kappa/d), T = \tilde{T}\cdot\beta\cdot d,\end{aligned} \tag{40}$$

with the constant depth d and the externally applied temperature gradient (32). Note that if the liquid is heated from below, $\beta < 0$. Introducing the deviation Θ from the thermally conducting state

$$\begin{aligned}T\left(\vec{r},t\right) &= T^0(z) + \Theta\left(\vec{r},t\right)\\ &= T_0 + \beta z + \Theta\left(\vec{r},t\right)\end{aligned} \tag{41}$$

transforms (20) into

$$\begin{aligned}\{\Delta - \partial_t\}\,\Theta\left(\vec{r},t\right) &= -\Lambda_2\Psi\left(\vec{r},t\right)\\ &\quad + \left(\vec{v}\cdot\nabla\right)\Theta\left(\vec{r},t\right)\end{aligned} \tag{42}$$

and (16) into

$$\left\{\Lambda - \frac{1}{\mathrm{Pr}}\partial_t\right\}\Lambda_2\Phi\left(\vec{r},t\right) = -\frac{1}{\mathrm{Pr}}\left[\mathrm{curl}\left(\left(\vec{v}\cdot\nabla\right)\vec{v}\right)\right]_z \tag{43a}$$

$$\begin{aligned}&\left\{\Lambda - \frac{1}{\mathrm{Pr}}\partial_t\right\}\Lambda\Lambda_2\Psi\left(\vec{r},t\right)\\ &= -R\,\Lambda_2\,\Theta\left(\vec{r},t\right) - \frac{1}{\mathrm{Pr}}\left[\mathrm{curl}\,\mathrm{curl}\left(\left(\vec{v}\cdot\nabla\right)\vec{v}\right)\right]_z.\end{aligned} \tag{43b}$$

Two dimensionless numbers occurred. One is the material dependent *Prandtl number*

$$\mathrm{Pr} = \frac{\nu}{\kappa}, \tag{44}$$

which measures the ratio of the diffusion times of heat and momentum. The other one is called the *Rayleigh number* and turns out to be

$$R = -\frac{\beta g \alpha d^4}{\nu\kappa} \tag{45}$$

with α defined in (36). The system (42) and (43) constitutes the basic equations for the three scalar fields, Φ, Ψ, and Θ which describe convective motion and temperature of a plane fluid layer with a flat and undeformable surface onto a plane substrate. This can be further simplified by taking the large Prandtl number limes $1/\mathrm{Pr} = 0$ (good for fluids with high viscosity, oils, etc.). Then Φ vanishes everywhere and only two equations are left:

$$\Delta^2 \Psi\left(\vec{r},t\right) = -R\,\Theta\left(\vec{r},t\right) \tag{46a}$$

$$\{\Delta - \partial_t\}\Theta\left(\vec{r},t\right) = -\Delta_2 \Psi\left(\vec{r},t\right) + \left(\vec{v}\cdot\nabla\right)\Theta\left(\vec{r},t\right). \tag{46b}$$

A general nonlinear (2D) solution of Eqs. (46) may be expressed by

$$\begin{bmatrix}\Psi(x,z,t)\\ \Theta(x,z,t)\end{bmatrix} = \sum_l \int_{-\infty}^{\infty} \mathrm{d}k\,\xi_l(k,t)\begin{bmatrix} f_l\left(k^2,z\right)\\ g_l\left(k^2,z\right)\end{bmatrix} e^{-ikx} \tag{47}$$

and

$$\xi_l(k,t) = \xi_l^*(-k,t)$$

where f and g are eigenfunctions of the ODE eigenvalue problem

$$\begin{aligned}\left(d_z^2 - k^2\right) f_l + R\, g_l &= 0\\ \left(d_z^2 - k^2 - \lambda_l\left(k^2\right)\right) g_l - k^2 f_l &= 0.\end{aligned} \tag{48}$$

Here, l labels the different eigenfunctions. Equation (48) is obtained by inserting (47) with $\xi_l \sim \exp.(\lambda t)$ into (46) and keeping only linear terms. The functions f_l and g_l can be calculated numerically by a finite difference method in vertical direction where suitable boundary conditions must be implemented.

Inserting (47) into (46) yields, after multiplication with the adjoint function g_l^+ exp. (ikx) and integration over the spatial coordinates, the system:

$$\begin{aligned}\partial_t \xi_l(k,t) &= \lambda_l\left(k^2\right)\xi_l(k,t)\\ &-\sum_{l'l''}\int_{-\infty}^{\infty} \mathrm{d}k'\,\mathrm{d}k''\, c_{ll'l''}(kk'k'')\,\xi_{l'}(k',t)\,\xi_{l''}(k'',t)\\ &\qquad \delta(k-k'-k''),\end{aligned} \tag{49}$$

where the coefficients c are matrix elements that can be computed directly from the basic equations for any given set of control parameters:

$$\begin{aligned}&c_{ll'l''}(kk'k'')\\ &\equiv k'^2\int_0^1 \mathrm{d}z\, g_l^+\left(k^2,z\right) f_{l'}\left(k'^2,z\right)\partial_z g_{l''}\left(k''^2,z\right)\\ &-k'k''\int_0^1 \mathrm{d}z\, g_l^+\left(k^2,z\right) g_{l'}\left(k'^2,z\right)\partial_z f_{l''}\left(k''^2,z\right).\end{aligned} \tag{50}$$

Here we are still at the same level of complexity; the infinitely many degrees of freedom intrinsic in the basic partial differential equations are expressed by an infinite number of mode amplitudes $\xi_l(k, t)$. To eliminate the fast damped modes by the linearly growing ones, we divide the eigenmodes into two groups:

$$\lambda_l \to \begin{cases}\lambda_u\left(k^2\right) \approx 0 \Rightarrow \xi_u(k,t)\\ \qquad\qquad |\,k\,| \approx k_c, u = l = 1\\ \lambda_s\left(k^2\right) \ll 0 \Rightarrow \xi_s(k,t)\\ \quad s = l > 1 \text{ or } s = l = 1 \text{ but } |k| \neq k_c.\end{cases} \tag{51}$$

In the following we may therefore substitute the index l by u (unstable) or s (stable), depending on the values of l and $|k|$. Now we express the amplitudes of the enslaved modes invoking an adiabatic

elimination (k_c denotes the wave vector that maximizes λ_u). In this case, the dynamics of the enslaved modes are neglected, they follow instantaneously to the order parameters. This is a special case of the slaving principle of *synergetics,* which can be used in many other disciplines beyond hydrodynamics (Haken 1983).

The remaining equations for the order parameters ξ_u, the amplitude equations, read (here and in the following we suppress the index u at ξ and λ):

$$\begin{aligned}\partial_t \xi(k,t) &= \lambda\left(k^2\right)\xi(k,t)\\ &+\int \mathrm{d}k'\mathrm{d}k''\mathrm{d}k'''\, B\left(k,k',k'',k'''\right)\xi(k',t)\xi(k'',t)\\ &\quad \xi\left(k''',t\right)\delta\left(k-k'-k''-k'''\right)\end{aligned} \tag{52}$$

where $|k|, |k'|, |k''|, |k'''| \approx |k_c|$. Note that there are no quadratic expressions in ξ. This is because $k - k' - k''$ cannot vanish if all wave numbers have the same (nonzero) absolute value. In three spatial dimensions this is different. Three k-vectors can then form a resonant triangle, which is the reason why stable hexagons may occur.

The Landau coefficient B is directly related to the matrix elements (50):

$$\begin{aligned}B\left(k,k',k'',k'''\right) &= \sum_s \frac{1}{\lambda_s\left(\left(k''+k'''\right)^2\right)}\\ c_{suu}\left(k''+k''',k',k''\right)&\left[c_{uus}\left(k,k',k''+k'''\right)\right.\\ &\left.+c_{usu}\left(k,k''+k''',k'\right)\right]\end{aligned}$$

where the indices u and s are defined in (51).

To arrive at the Ginzbur–Landau equation, one must transform back to real space. If we express the δ-function in (52) as

$$\delta\left(k-k'-k''-k'''\right) = \frac{1}{2\pi}\int \mathrm{d}x\, \mathrm{e}^{i\left(k-k'-k''-k'''\right)x}$$

and assume, that the coefficient B does not depend much on k (it can be evaluated at $k = \pm k_c$), the cubic part of (52) takes the form

$$\begin{aligned}&\frac{\overline{B}}{2\pi}\int \mathrm{d}x \mathrm{e}^{ikx}\int \mathrm{d}k'\,\xi(k',t)\,\mathrm{e}^{-ik'x}\int \mathrm{d}k''\xi(k'',t)\\ &\mathrm{e}^{-ik''x}\int \mathrm{d}k'''\,\xi\left(k''',t\right)\mathrm{e}^{-ik'''x}\\ &\qquad = \frac{\overline{B}}{2\pi}\int \mathrm{d}x\, \mathrm{e}^{ikx}\Psi^3(x,t)\end{aligned} \tag{53}$$

where we have introduced the Fourier transform

$$\Psi(x,t) = \int \mathrm{d}k\,\xi(k,t)\,\mathrm{e}^{-ikx}. \tag{54}$$

Inserting (53) into (52), multiplying with $\mathrm{e}^{-ik\widetilde{x}}$ and integrating over k yields the order parameter equation in real space

$$\begin{aligned}\partial_t \Psi(\widetilde{x},t) &= \int \mathrm{d}k\lambda(k)\,\xi(k,t)\,\mathrm{e}^{-ik\widetilde{x}}\\ &\quad +\overline{B}\,\Psi^3(\widetilde{x},t).\end{aligned} \tag{55}$$

If we replace the k^2 -dependence of λ under the integral by $-\partial^2_{\widetilde{xx}}$ we may pull A out of the integral and write (55) in the form

$$\partial_t \Psi(x,t) = \lambda\left(-\partial^2_{xx}\right)\Psi(x,t) + \overline{B}\,\Psi^3(x,t). \tag{56}$$

The function $\Psi(x, t)$ can also be called an "order parameter", though it is not slowly varying in space compared to the small scale structure of the rolls, an idea which we shall work out in the following section. One big advantage can already be seen: the reduction of the number of space dimensions by one. We started with the hydrodynamic equations in two dimensions and get an order parameter equation in only one spatial dimension.

To find the form of the Ginzbur–Landau equation, we must introduce a slowly varying order parameter. This is done by recalling that the Fourier transform of W is mainly excited around $k = \pm k_c$. Then it is natural to make a "rotating wave approximation" with respect to x of the form

$$\Psi(x,t) = \xi(x,t)\,\mathrm{e}^{ik_c x} + \xi^*(x,t)\,\mathrm{e}^{-ik_c x}. \tag{57}$$

Inserting this into (56), multiplying by $\mathrm{e}^{-ik_c x}$ and integrating with respect to x over one period

$2\pi/k_c$ yields with the assumption of constant (slowly varying) ξ in this period

$$\partial_t \xi(x,t) = \lambda\left(-(\partial_x + ik_c)^2\right)\xi(x,t) + 3\overline{B}\,|\xi(x,t)|^2\xi(x,t).$$

The last approximation is concerned with the evaluation of the eigenvalue in form of a differential operator. Close to k_c, it has the form of a parabola, see Fig. 15 middle frame. Thus we may approximate

$$\lambda\left(k^2\right) = \varepsilon - q^2\left(k^2 - k_c^2\right)^2 \tag{58}$$

and also

$$\begin{aligned}\lambda\left(-(\partial_x + ik_c)^2\right) &= \varepsilon - q^2\left((\partial_x + ik_c)^2 + k_c^2\right)^2 \\ &= \varepsilon - q^2\left(\partial_{xx}^2 + 2ik_c\partial_x\right)^2 \\ &\approx \varepsilon + 4q^2k_c^2\partial_{xx}^2.\end{aligned} \tag{59}$$

For the last conversion, we neglect higher derivatives, which is justified due to the slowly varying spatial dependence of ξ. After scaling of ξ and the additional assumption $\overline{B} < 0$ we finally have derived the Ginzbur–Landau Eq. (39).

The Swift-Hohenberg Equation

In two spatial dimensions, the drawback of the Ginzburg-Landau equation is its lack of rotational symmetry. Therefore, it is better to pass on the rotating wave approximation (57) and to consider instead the fully space-dependent function Ψ as an order parameter, but now in two spatial dimensions. The resulting evolution equation in its lowest nonlinear approximation is the Swift-Hohenberg Eq. (88)

$$\dot{\Psi}\left(\vec{x},t\right) = \left[\varepsilon - (1+\Delta_2)^2\right]\Psi\left(\vec{x},t\right) - \Psi^3\left(\vec{x},t\right), \tag{60}$$

which we shall derive now.

Non-local Order Parameter Equations To this end we go back to (52) and write it down in two dimensions, now including the quadratic terms $\left(\vec{k} = (k_x, k_y)\right)$:

$$\begin{aligned}\partial_t\xi\left(\vec{k},t\right) &= \lambda\left(k^2\right)\xi\left(\vec{k},t\right) + \int \mathrm{d}^2\vec{k}'\,\mathrm{d}^2\vec{k}''\,A\left(\vec{k},\vec{k}',\vec{k}''\right) \\ &\cdot\xi\left(\vec{k}',t\right)\xi\left(\vec{k}'',t\right)\delta\left(\vec{k}-\vec{k}'-\vec{k}''\right) + \int \mathrm{d}^2\vec{k}'\,\mathrm{d}^2\vec{k}''\,\mathrm{d}^2\vec{k}''' \\ &\cdot B\left(\vec{k},\vec{k}',\vec{k}'',\vec{k}'''\right)\xi\left(\vec{k}',t\right)\xi\left(\vec{k}'',t\right)\xi\left(\vec{k}''',t\right) \\ &\cdot\delta\left(\vec{k}-\vec{k}'-\vec{k}''-\vec{k}'''\right).\end{aligned} \tag{61}$$

Introducing the (2D) Fourier transform $\left(\vec{x} = (x,y)\right)$,

$$\Psi\left(\vec{x},t\right) = \int \mathrm{d}^2\vec{k}\,\xi\left(\vec{k},t\right)\mathrm{e}^{-i\vec{k}\vec{x}}. \tag{62}$$

and transforming (61) to real space yields the integro-differential equation

$$\begin{aligned}&\partial_t\Psi\left(\vec{x},t\right) = \lambda(\Delta)\Psi\left(\vec{x},t\right) \\ &+\int\int \mathrm{d}^2\vec{x}'\,\mathrm{d}^2\vec{x}''\,G^{(2)}\left(\vec{x}-\vec{x}',\vec{x}-\vec{x}''\right)\Psi\left(\vec{x}',t\right)\Psi\left(\vec{x}'',t\right) \\ &+\int\int\int \mathrm{d}^2\vec{x}'\,\mathrm{d}^2\vec{x}''\,d^2\vec{x}'''\,G^{(3)}\left(\vec{x}-\vec{x}',\vec{x}-\vec{x}'',\vec{x}-\vec{x}'''\right) \\ &\Psi\left(\vec{x}',t\right)\Psi\left(\vec{x}'',t\right)\Psi\left(\vec{x}''',t\right)\end{aligned} \tag{63}$$

where the kernels are computed by the Fourier transforms:

$$\begin{aligned}&G^{(2)}\left(\vec{x},\vec{x}'\right) \\ &\quad= \frac{1}{16\pi^4}\int \mathrm{d}^2\vec{k}\,\mathrm{d}^2\vec{k}'\,A\left(\vec{k}+\vec{k}',\vec{k},\vec{k}'\right)\mathrm{e}^{-i\vec{k}\vec{x}}\,\mathrm{e}^{-i\vec{k}'\vec{x}'}, \\ &G^{(3)}\left(\vec{x},\vec{x}',\vec{x}'''\right) \\ &\quad= \frac{1}{64\pi^6}\int \mathrm{d}^2\vec{k}\,\mathrm{d}^2\vec{k}'\,\mathrm{d}^2\vec{k}''\,B\left(\vec{k}+\vec{k}'+\vec{k}'',\vec{k},\vec{k}',\vec{k}''\right) \\ &\qquad\cdot\mathrm{e}^{-i\vec{k}\vec{x}}\,\mathrm{e}^{-i\vec{k}'\vec{x}'}\,\mathrm{e}^{-i\vec{k}''\vec{x}''}.\end{aligned} \tag{64}$$

Gradient Expansion Although Eq. (63) has a rather general form, its further numerical treatment is not practicable, at least not in two dimensions. Each integral must be approximated somehow as a sum over mesh points. The cubic coefficients would result in a 6-fold sum with, if N is the number of mesh points, N^6 summands, which is, if N is around the size of 100, rather hopeless.

On the other hand, the excitation of ξ mainly close to k_c, in two dimensions on a (narrow) ring in Fourier space with radius k_c, makes it natural to expand Ψ under the integrals around $\vec{x}$. This works well if the kernels (64) have a finite (small) range with significant contribution only for $|\vec{x} - \vec{x}'| < \Lambda$ with $\Lambda = 2\pi/k_c$.

To save space we demonstrate the method only for the quadratic term of (63) and in one spatial dimension. A Taylor expansion of Ψ leads to

$$\int\int \mathrm{d}x'\mathrm{d}x'' G^{(2)}(x-x', x-x'') \sum_{m,n=0}^{\infty} \frac{1}{m!n!} \frac{\partial^m \Psi}{\partial x^m} \frac{\partial^n \Psi}{\partial x^n} (x-x')^m (x-x'')^n,$$

where the derivatives must be evaluated at x. They can be written in front of the integrals, yielding

$$\sum_{m,n=0}^{\infty} g^{(2)}_{m\,n} \frac{\partial^m \Psi}{\partial x^m} \frac{\partial^n \Psi}{\partial x^n} \tag{65}$$

with the moments

$$g^{(2)}_{mn} = \frac{1}{m!n!} \int\int \mathrm{d}x_1\, \mathrm{d}x_2\, G^{(2)}(x_1, x_2) x_1^m x_2^n).$$

A similar expression can be found for the cubic coefficient. A series of the form (65) is called *gradient expansion.* In this way, a local order parameter equation results, but which now has infinitely many nonlinear terms. It reads

$$\partial_t \Psi = \lambda(\Delta)\Psi + \sum_{m,n=0}^{\infty} g^{(2)}_{mn} \frac{\partial^m \Psi}{\partial x^m} \frac{\partial^n \Psi}{\partial x^n} + \sum_{l,m,n=0}^{\infty} g^{(3)}_{l\,m\,n} \frac{\partial^l \Psi}{\partial x^l} \frac{\partial^m \Psi}{\partial x^m} \frac{\partial^n \Psi}{\partial x^n} \tag{66}$$

with

$$g^{(3)}_{lmn} = \frac{1}{l!m!n!} \int\int\int \mathrm{d}x_1\, \mathrm{d}x_2\, \mathrm{d}x_3\, G^{(3)}(x_1, x_2, x_3) x_1^l x_2^m x_3^n.$$

For more details see (Bestehorn and Friedrich 1999).

Swift-Hohenberg-Haken Equation The series in (66) will converge rapidly if the kernels have a short range. Here we consider only the extreme case of δ-shaped kernels, now in two dimensions:

$$G^{(2)}\left(\vec{x}_1, \vec{x}_2\right) = A \cdot \delta\left(\vec{x}_1\right)\delta\left(\vec{x}_2\right),$$

$$G^{(3)}\left(\vec{x}_1, \vec{x}_2, \vec{x}_3\right) = B \cdot \delta\left(\vec{x}_1\right)\delta\left(\vec{x}_2\right)\delta\left(\vec{x}_3\right).$$

All coefficients vanish, except $g^{(2)}_{00}$ and $g^{(3)}_{000}$. Then (66) simplifies to

$$\partial_t \Psi\left(\vec{x}, t\right) = \lambda(\Delta)\Psi\left(\vec{x}, t\right) + A\,\Psi^2\left(\vec{x}, t\right) + B\,\Psi^3\left(\vec{x}, t.\right). \tag{67}$$

For the linear part we again use the expansion (58) and replace k^2 by $-\Delta$. After rescaling of length, time and V, (67) turns into the canonical form

$$\dot{\Psi}\left(\vec{x}, t\right) = \left[\varepsilon - (1 + \Delta_2)^2\right]\Psi\left(\vec{x}, t\right) + a\,\Psi^2\left(\vec{x}, t\right) - \Psi^3\left(\vec{x}, t\right) \tag{68}$$

With

$$a = \frac{A}{\sqrt{-B}}.$$

Equation (68) is the Swift–Hohenberg–Haken equation derived first using the theoretical methods of synergetics by Haken (Bestehorn and Haken 1983; Haken 1983).

Numerical solutions of (68) with $a = 0$ are shown in Fig. 18. Stripes as known from convection, but also from Turing instabilities, can be clearly seen. If $|a|$ exceeds a certain value which depends on $\sqrt{\varepsilon}$, hexagonal structures are found which agree qualitatively with those obtained in Bénard–Marangoni convection (Fig. 19). It can be shown that the symmetry break $z \to -z$ caused by the different vertical boundary conditions on top and bottom of the fluid gives rise to a (positive) quadratic coefficient. In the Swift–Hohenberg equation, this violates the symmetry $\Psi \to -\Psi$ and may stabilize two different sorts of hexagons, namely the already mentioned l - and g - hexagons. The first ones are found for large enough positive a, the latter for negative a.

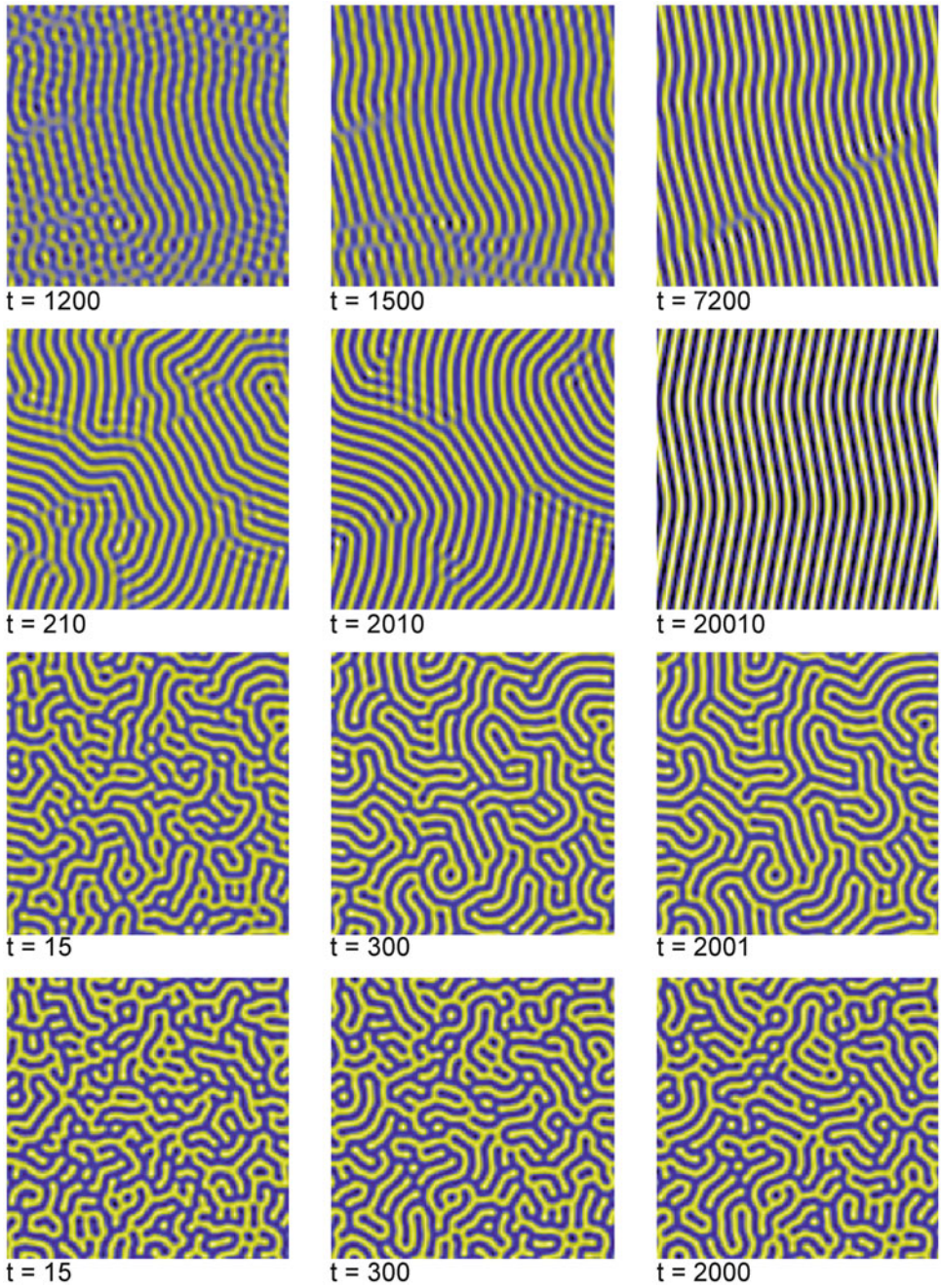

Fluid Dynamics, Pattern Formation, Fig. 18 Computer solutions of the Swift–Hohenberg Eq. (60) for several $\varepsilon = 0.01, 0.1, 1.0, 2.0$ (*top to bottom*). The evolution time scales with $1/\varepsilon$, the number of defects increases with ε

The Swift–Hohenberg equation can be considered as normal form of type I_s instabilities. The bifurcation scenario is general (Fig. 20): hexagons are the generic form at onset if symmetry breaking (quadratic) terms occur, which is normal. Even very small symmetry breaking effects lead to hexagons, although their stability region will decrease and finally shrink to the critical point

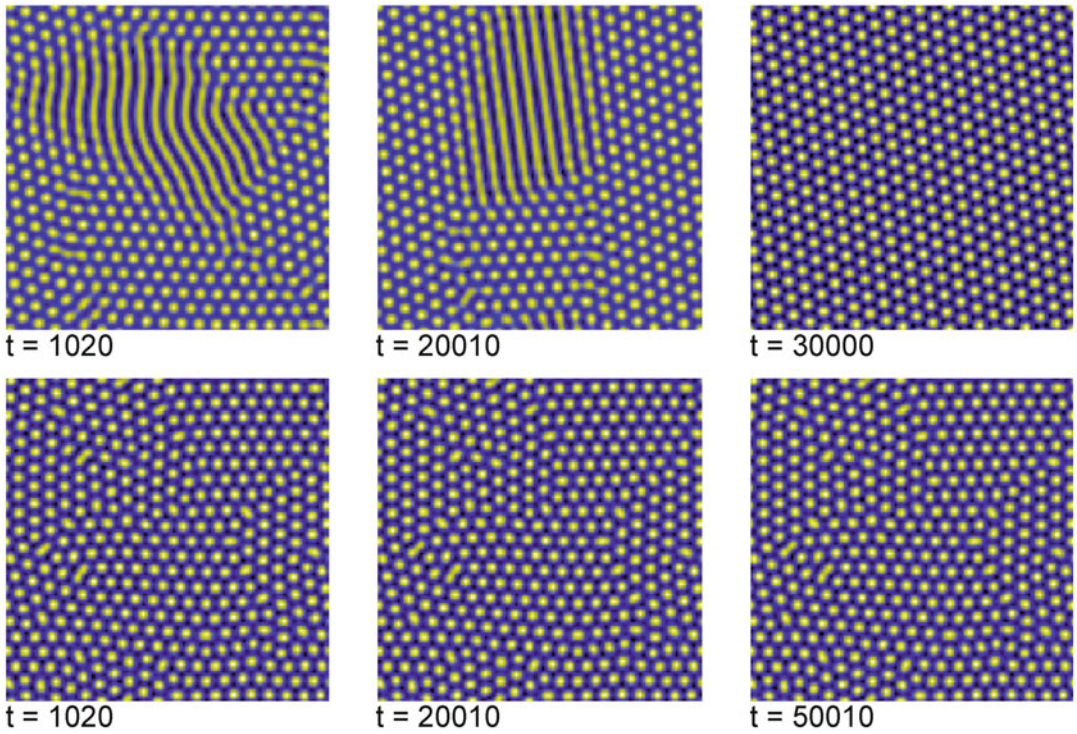

Fluid Dynamics, Pattern Formation, Fig. 19 Evolution of a random dot initial condition from (68) with $\varepsilon = 0.1$, $a = 0.26$ (*top*) and $a = 1.3$ (*bottom*). For a in the bistable region, top row, stripes and hexagons coexist for a long time until hexagons win. *Bottom:* for rather large a hexagons are formed soon showing many defects and grain boundaries. The defects survive for quite a long time

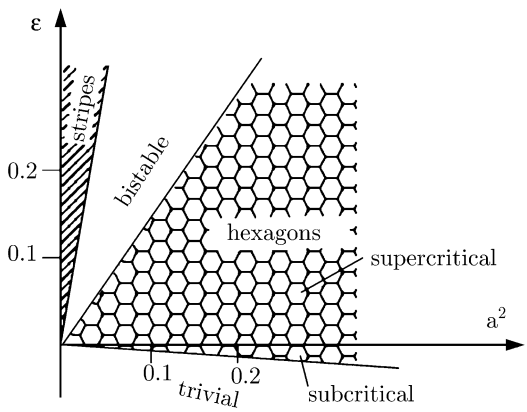

Fluid Dynamics, Pattern Formation, Fig. 20 Stability regions in the parameter plane of Eq. (68). Hexagons bifurcate subcritically from the trivial solution $\Psi = 0$. As a secondary instability, stripes emerge. The transition hexagons-stripes as well as trivial sol-hexagons both show hysteresis

$\varepsilon = 0$ if $a \to 0$. Well above threshold, stripes are expected – or squares.

Squares A linear stability analysis of the Swift–Hohenberg Eq. (68) shows that squares are always unstable in favor of rolls (or hexagons). Therefore there exists no stable square pattern as a solution. This can be changed including higher order terms in the gradient expansion (66), for details see (Bestehorn and Pérez-García 1992). In this spirit, the equation

$$\partial_t \Psi = \varepsilon \Psi - (\Delta + 1)^2 \Psi - b\, \Psi^3 - c\, \Psi \Delta^2 (\Psi^2) \tag{69}$$

has a stable square solution for $-32c/9 < b < 0$. In Fig. 21 we present numerical solutions of (69) for two different values of the parameter b.

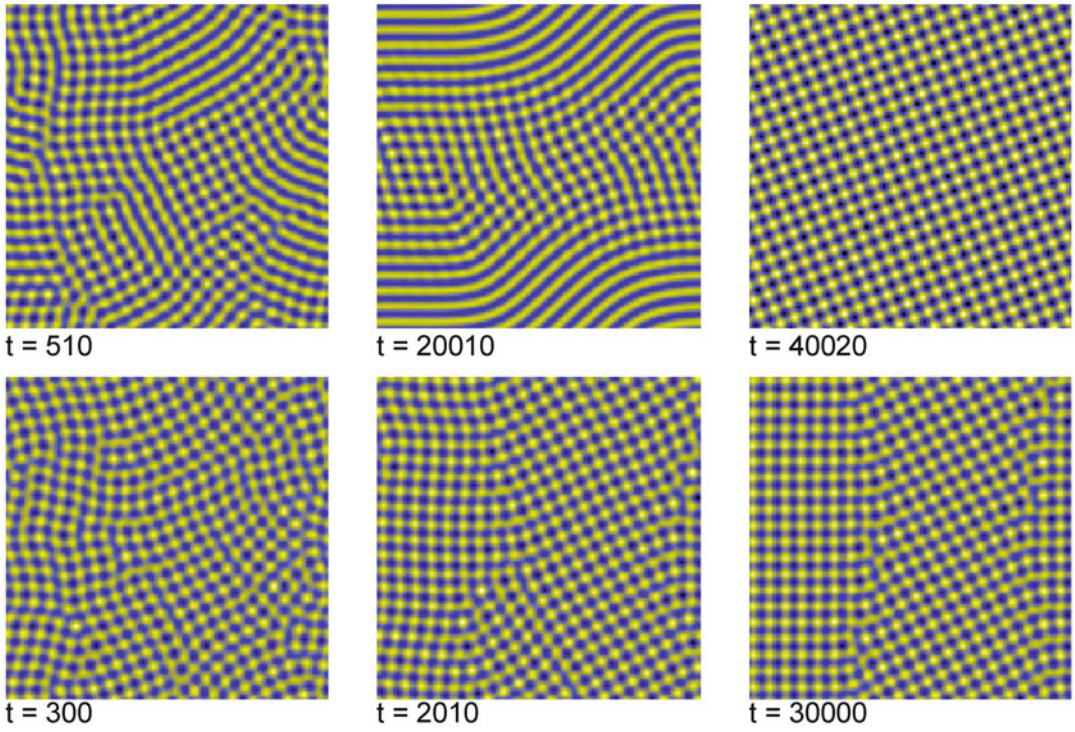

Fluid Dynamics, Pattern Formation, Fig. 21 Numerical solutions of (69) for e = 0.1, $c = 1/16$ and $b = 0$ (*top*), $b = -0.1$ (*bottom*). For $b = 0$ both squares and stripes are stable. After a longer time squares win the competition. *Bottom:* clearly in the square region of parameter space. Squares are formed soon having many defects and grain boundaries. Finally, a rather regular square pattern evolves

Regular squares are found in convection experiments with two poorly conducting top and bottom plates (Busse and Riahi 1980) or in binary mixtures with a certain mean concentration (Moses and Steinberg 1986). If the fluid viscosity is strongly temperature dependent (non-boussinesq effects), squares are also preferred, as shown in (Busse and Frick 1985). For all these cases, an equation of the form (69) can be approximately derived close to onset.

Conserved Order Parameter Fields

In the previous section, the OPE had the general form

$$\partial_t \xi\left(\vec{r}, t\right) = F(\xi, \nabla\xi, \Delta\xi) \tag{70}$$

with no further restrictions (except of boundary conditions) for the order parameter field ξ. However, there are many cases where the physical meaning of the order parameter is that of a density belonging to a conserved quantity such as total mass, volume or charge. Let ξ be such a density; then the mean value

$$M = \langle F \rangle \equiv \frac{1}{V} \int_V \mathrm{d}^3\vec{r}\, F(\xi, \nabla\xi, \Delta\xi) \tag{71}$$

should vanish, if $\langle\xi\rangle$ is a conserved quantity in the constant volume V. Then F can be written as

$$F(\xi, \nabla\xi, \Delta\xi) = -\mathrm{div}\ \vec{j}\left(\vec{r}, t\right) \tag{72}$$

if the total flow of the current density $\vec{j}$ through the surface A of V vanishes

$$\oint_{A(V)} \mathrm{d}^2\vec{f} \cdot \vec{j}\left(\vec{r}, t\right) = 0. \tag{73}$$

With (72), Eq. (70) takes the form of a continuity equation. In this section we wish to consider OPEs that fulfill (72) and (73).

Thin Films

Consider a fluid with a free and deformable surface located at $z = h(x, y, t)$ as already shown in Fig. 3. If the fluid is incompressible and there is no flow through the sidewalls, the total volume of the fluid layer

$$A \cdot \langle h \rangle = \int_A \mathrm{d}x\, \mathrm{d}y\, h(x, y, t) \tag{74}$$

is a conserved quantity, where A is the base area of the layer. As a consequence, the evolution equation for h must have the form

$$\partial_t h = -\mathrm{div}\ \vec{j} = -\partial_x j_x - \partial_y j_y. \tag{75}$$

Comparing (75) with the kinematic boundary conditions (23) and taking $v_z|_{z=h}$ from the integral of the incompressibility condition (3)

$$v_z|_{z=h} = -\int_0^h \mathrm{d}z\, \left(\partial_x v_x + \partial_y v_y\right) + v_z|_{z=0}$$

one finds with $v_z|_{z=0} = 0$

$$\vec{j} = \int_0^h \mathrm{d}z\, \vec{v}_H, \tag{76}$$

where $\vec{v}_H$ denotes the two horizontal velocity components.

The Lubrication Approximation To close the Eqs. (75), (76), it is necessary to compute $\vec{v}_H$ as a function of h. For thin films, the Reynolds number is small and the Stokes Eq. (19) determines the fluid velocity to a good approximation. Using scaling (Oron et al. 1997)

$$x = \tilde{x} \cdot l, y = \tilde{y} \cdot l, z = \tilde{z} \cdot \mathrm{d}, t = \tilde{t} \cdot \tau, h = \tilde{h} \cdot \mathrm{d}, \tag{77}$$

(19) turns into

$$\left(\delta^2\left(\partial^2_{\tilde{x}\tilde{x}} + \partial^2_{\tilde{y}\tilde{y}}\right) + \partial^2_{\tilde{z}\tilde{z}}\right)\vec{\tilde{v}}_H = \tilde{\nabla}_2 \tilde{P} \tag{78a}$$

$$\delta^2\left(\delta^2\left(\partial^2_{\tilde{x}\tilde{x}} + \partial^2_{\tilde{y}\tilde{y}}\right) + \partial^2_{\tilde{z}\tilde{z}}\right)\tilde{v}_z = \partial_{\tilde{z}}\tilde{P}. \tag{78b}$$

with the 2D-gradient $\nabla_2 = (\partial_x, \partial_y)$. In (78) we have introduced the dimensionless velocity and pressure

$$\vec{v}_H = \vec{\tilde{v}}_H \cdot \frac{l}{\tau}, v_z = \tilde{v}_z \cdot \frac{d}{\tau}, P = \tilde{P} \cdot \frac{\eta}{\delta^2 \tau}$$

and $\delta = d/l$ as a small parameter already defined in (24). In the limit $\delta \to 0$ it follows from (78b)

$$\partial_{\tilde{z}}\tilde{P} = 0 \text{ or } \tilde{P} = \tilde{P}(\tilde{x}, \tilde{y}).$$

Thus one can integrate (78a) twice over h and finds with the no-slip condition $\vec{\tilde{v}}_H(0) = 0$

$$\vec{\tilde{v}}_H(\tilde{x}, \tilde{y}, \tilde{z}) = \vec{f}(\tilde{x}, \tilde{y}) \cdot \tilde{z} + \frac{1}{2}\left(\tilde{\nabla}_2 \tilde{P}(\tilde{x}, \tilde{y})\right) \cdot \tilde{z}^2 \tag{79}$$

with a function $\vec{f}(\tilde{x}, \tilde{y})$ which can be determined by the boundary conditions. To this end we consider an inhomogeneous surface tension (caused, for example, by a temperature gradient) at the free surface, which yields the condition

$$\eta\, \partial_z \vec{v}_H|_{z=h} = \nabla_2 \Gamma|_{z=h}.$$

Inserting (79) there one finds

$$\vec{f} = \tilde{\nabla}_2 \tilde{\Gamma} - \left(\tilde{\nabla}_2 \tilde{P}\right) \cdot \tilde{h}$$

with the non-dimensional surface tension

$$\tilde{\Gamma} = \Gamma \frac{\tau d}{\eta l^2}.$$

Inserting everything into (76) and integrating by $\tilde{z}$ finally yields (all tildes omitted)

$$\partial_t h = -\nabla_2\left[-\frac{h^3}{3}\nabla_2 P + \frac{h^2}{2}\nabla_2 \Gamma\right]. \tag{80}$$

This is the basic equation for the evolution of the surface of a thin film in the so-called lubrication approximation (Ockendon and Ockendon 1995). Eq. (80) is sometimes denoted as the *thin film equation* (Oron et al. 1997; Vrij 1966).

The Disjoining Pressure for Ultra-thin Films Gravitation and surface tension can be included into the pressure P as already outlined in Section "Surface Waves". They both stabilize the flat film. On the other hand, an instability mechanism is encountered in very thin (ultra-thin) films where the thickness is some 100 nm or even less

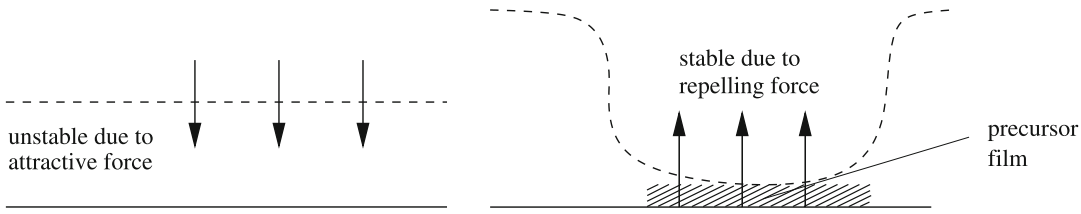

Fluid Dynamics, Pattern Formation, Fig. 22 Left: Thin flat films are unstable due to an attractive, long range van der Waals force between the free surface and the solid substrate of the fluid. *Right:* If the film is extremely thin (some nm), a repelling short range force acts as a stabilizer and the precursor film remains intact instead of rupturing

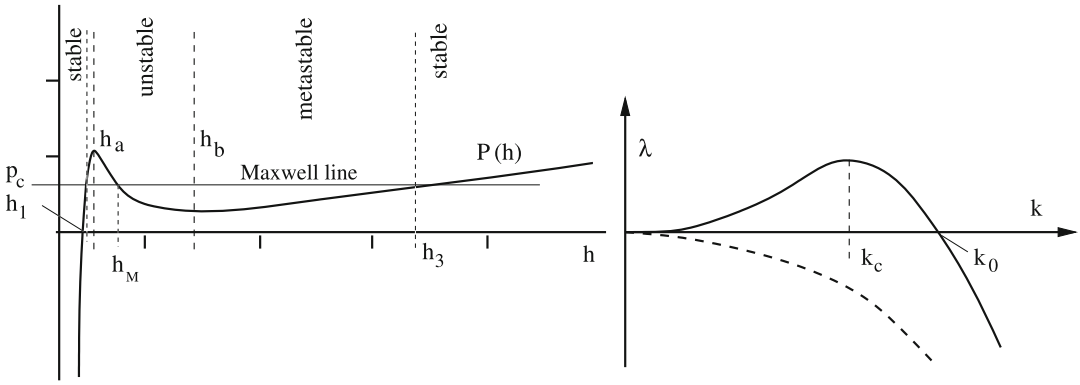

Fluid Dynamics, Pattern Formation, Fig. 23 *Left:* The disjoining pressure for a film with uniform thickness h including gravitation, $A_3 = 3$, $A_9 = 1$, $G = 0.1$. The region of unstable films is bounded by h_a and h_b. The critical pressure (depth) P_c (h_M) where drops turn into holes is determined by a Maxwell construction. *Right:* Growth rates of periodic disturbances of the plane surface with wave number k. The solid line corresponds to a film with a mean thickness in the unstable regime. Waves having a wave number $0 < k < k_0$ grow exponentially, the mode with $k = k_c$ has the largest growth rate (most dangerous mode). The instability is of type II

(Israelachvili 1992; Reiter et al. 1999; Sharma and Khanna 1998). Then, van der Waals forces between free surface and solid substrate can no longer be neglected (Israelachvili 1992). For an attractive force between surface and substrate one has

$$d_h P < 0.$$

But there can also exist a repelling van der Waals force with $d_h P > 0$ which stabilizes the flat surface. Attractive and repelling forces have different ranges. Usually, the repelling force is short range, the attractive one long range. Then, the initially "thick" film can be unstable due to attraction but rupture is avoided by repulsion. In this way completely dry regions cannot exist but the substrate always remains covered by an extremely thin film (some nm), called *precursor film,* Fig. 22 (Hardy 1919).

The complete expression for such an attractive/repulsive disjoining pressure including gravity and surface tension would be (Fig. 23)

$$P(h) = \frac{A_3}{h^3} - \frac{A_9}{h^9} + Gh - q\,\Delta_2\,h \qquad (81)$$

where A_3 and A_9 are material parameters, the Hamaker constants, and

$$G = \frac{d^3 g \tau}{l^2 \nu}, \quad q = \Gamma \frac{\tau d^3}{l^4 \eta}$$

denote the dimensionless gravitation number and the surface tension, respectively.

Spinodal Dewetting – Numerical Results If a thin liquid film is exposed to a non-or partially wetting substrate, a small perturbance is sufficient to destabilize the flat surface. The fluid then bubbles and many small drops are formed. This

phenomenon can be seen for instance if rain falls on a waxed cloth or on a well polished car roof. Such a process is called *spinodal dewetting* and refers to the unstable region of Fig. 23, (Bestehorn and Neuffer 2001; Seemann et al. 2001). As already explained in Section "Instabilities", an instability of the flat film occurs in the region where P has a negative slope. This instability is of type II, as is shown in Fig. 23, right frame, and has the growth rate (dispersion relation)

$$\lambda = \frac{1}{3}h_0^3\left(-D(h_0)k^2 - k^4\right) \tag{82}$$

with the "diffusion coefficient"

$$D(h) = d_h P.$$

(Here we restrict our further study to fluids with a uniform surface tension. For non-isothermal films with $\nabla_2 \Gamma \neq 0$ we refer to (Bestehorn et al. 2003; Oron 2000)). Next we wish to present numerical solutions of the fully nonlinear Eq. (80) with (81). To this end we used the parameters of Fig. 23 and several initial depths h_0. As initial condition a random distribution around the average depth h_0 was chosen.

In the early stage of the evolution (top line of Fig. 24), structures having a length scale of the critical wave length $\Lambda = 2\pi/k_c$, occur, were k_c is the wave number of the fastest growing mode

$$k_c = \sqrt{-\frac{D}{2}}.$$

This can be called "linear phase" since the amplitudes are still small and nonlinearities play no important role. The structure grows on the typical time scale

$$\tau = \lambda^{-1}(k_c) = \frac{12}{h_0^3 D^2} = \frac{12}{h_0^3}\left(P'(h_0)\right)^{-2},$$

which is inverse to the square of the slope of the disjoining pressure. This is the reason why pattern formation in thicker films takes much longer (right column in Fig. 24). As a consequence, the small scale (linear phase) structures are overlayed by holes created by certain seeds. After the linear phase, the position of h_0 with respect to the Maxwell point h_M (Fig. 23, left frame) is decisive. If $h_0 > h_M$, holes are formed, for $h_0 < h_M$, one finds drops. If $h_0 \approx h_M$, maze-like patterns are obtained in form of bent, rather irregular stripes (Fig. 24, middle column). In a last, strongly nonlinear phase, coarsening is observed. The final stationary structure (long term) is often a single entity in the form of one big drop or hole. The whole spatio-temporal evolution is transient and can be formulated as a gradient dynamics. The potential plays the role of a generalized free energy reaching its minimum in the steady end state (Bestehorn et al. 2003).

The flat film is unstable with respect to infinitesimal disturbances if h_0 is in the region between h_a and h_b. On the other hand, two meta-stable domains exist, where the flat film is stable, although the free energy could be lowered by pattern formation. Then, a finite disturbance is necessary, which can be caused by seeds coming, for instance, from impurities. Such a process is called *nucleation* and can be seen in the right column of Fig. 24. There, the seeds were provided by the random dot initial conditions and two holes are formed. Both processes (nucleation and wetting) converge in this region and it is a question of time scales which one emerges first. In experiments, the formation of holes by nucleation is seen quite often. The reason is that for a Lennard–Jones like disjoining pressure as (81), the meta-stable hole region is much larger compared to that of drops (Fig. 23, left frame).

Phase Field Models

In solidification processes, phase fields are introduced as additional variables to describe the state, here liquid or solid, of the system (Langer 1980). Phase fields depend on space and time and governing equations for the phase field variables must be stated or derived. If the phase field obeys an equation of the form of (70), it is called Model A, according to a classification given by Hohenberg and Halperin (Hohenberg and Halperin 1977).

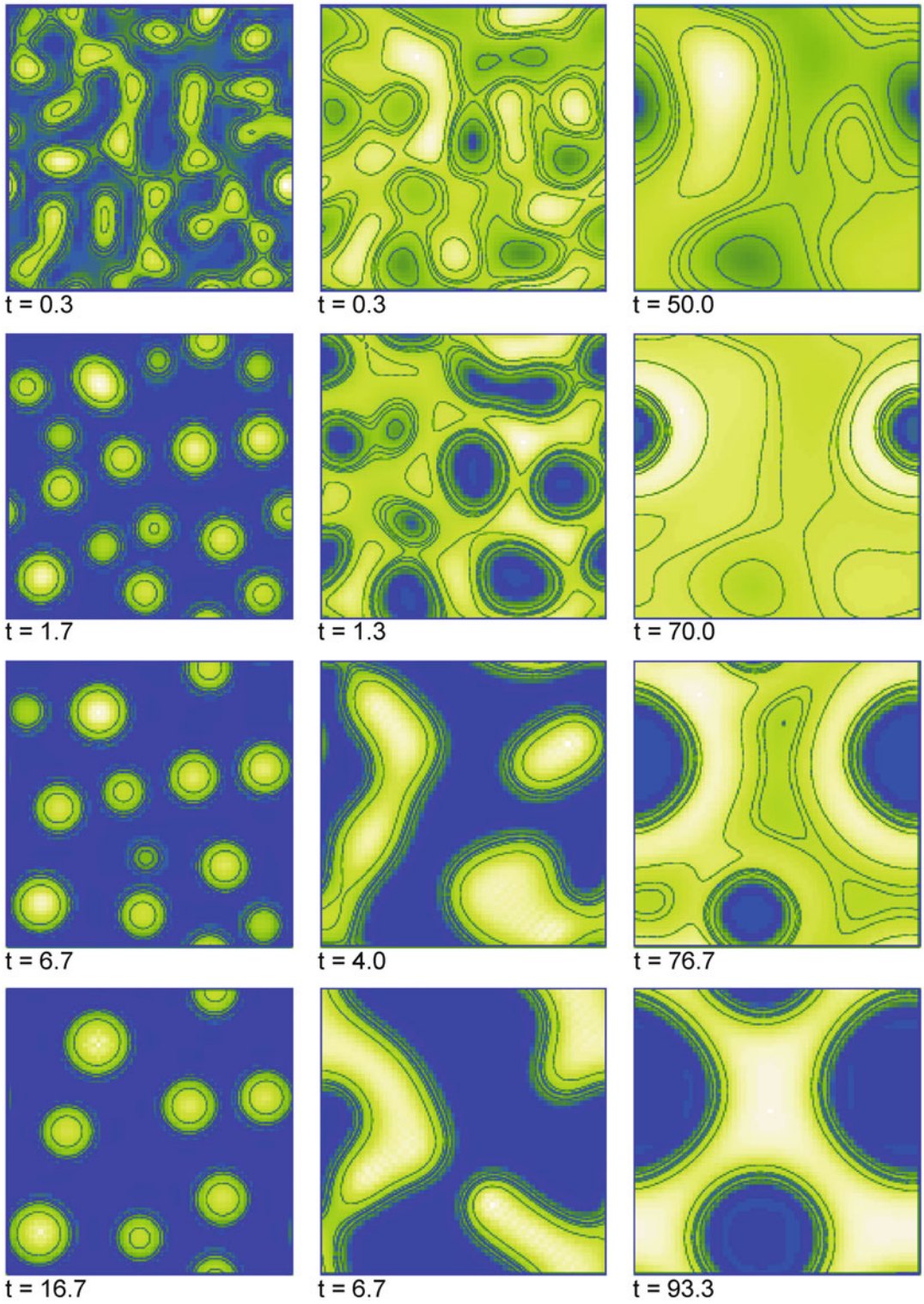

Fluid Dynamics, Pattern Formation, Fig. 24 Time series found by numerical integration of (80) for $h_0 = 1.2$ (*left column*), 1.862 (*middle*), and 2.8 (*right*). Light areas correspond to elevated regions of the surface (from Bestehorn 2007)

Model B Here, we are more interested in phase field equations belonging to Model B. The phase field (we call it Φ) is conserved and a continuity equation

$$\partial_t \Phi = -\mathrm{div}\ \vec{j} \tag{83}$$

must hold. As in nonequilibrium thermodynamics (Callen 1985) one assumes that the current density $\vec{j}$ is proportional to a generalized force $\vec{f}$

$$\vec{j} = Q(\Phi) \cdot \vec{f} \tag{84}$$

where Q stands for a non-negative mobility, which is normally a function of the phase field itself, but may also explicitly depend on space coordinates. If the force can be derived from a potential P (pressure)

$$\vec{f} = -\nabla P(\Phi) \tag{85}$$

which in turn can be written as functional derivative of another (thermodynamic) potential (free energy) F

$$P = \frac{\delta F}{\delta \Phi}, \tag{86}$$

we finally obtain a closed equation for (83) of the form

$$\partial_t \Phi = \mathrm{div}\left[Q(\Phi) \nabla \frac{\delta F}{\delta \Phi} \right]. \tag{87}$$

With (87) it is easy to show that $\mathrm{d}_t F \leq 0$.

The Cahn-Hilliard Equation As known from the Ginzbur–Landau equation, one may expand the free energy with respect to powers of the phase field. The surface term $(\nabla\Phi)^2$ penalizes phase field variations with respect to space by an increase of F:

$$F[\Phi] = \int_V d^3\vec{r} \left[\frac{D}{2} (\nabla\Phi)^2 + a_0 \Phi + \frac{a_1}{3} \Phi^2 + \frac{a_2}{3} \Phi^3 + \frac{a_3}{4} \Phi^4 + \ldots \right]. \tag{88}$$

Substituting this into (87) yields

$$\partial_t \Phi = \mathrm{div}[Q(\Phi) \nabla (-D\Delta\Phi + a_0 + a_1 \Phi) + a_2 \Phi^2 + a_3 \Phi^3]. \tag{89}$$

We further assume $a_2 = 0$ (this can be always obtained by a simple shift of Φ) and $a_1 < 0$, $a_3 > 0$. If we restrict us to the case of a constant mobility, we arrive from (89) after a suitable scaling at the Cahn-Hilliard Eq. [29]

$$\partial_t \Phi = -\Delta\Phi - \Delta^2 \Phi + \Delta(\Phi^3). \tag{90}$$

Equation (90) can be considered as a simple model for a conserved order parameter. A family of stationary solutions of (90) is given by $\Phi = \Phi_0 =$ constant. A linear stability analysis shows that these solutions are type II unstable if $\Phi_0^2 < \frac{1}{3}$ holds. Since (90) belongs to Model B, an infinitesimal disturbance can grow only in a way that keeps the mean value of $\Phi = \Phi_0$ constant. Therefore, spatially structured solutions are expected (Fig. 25).

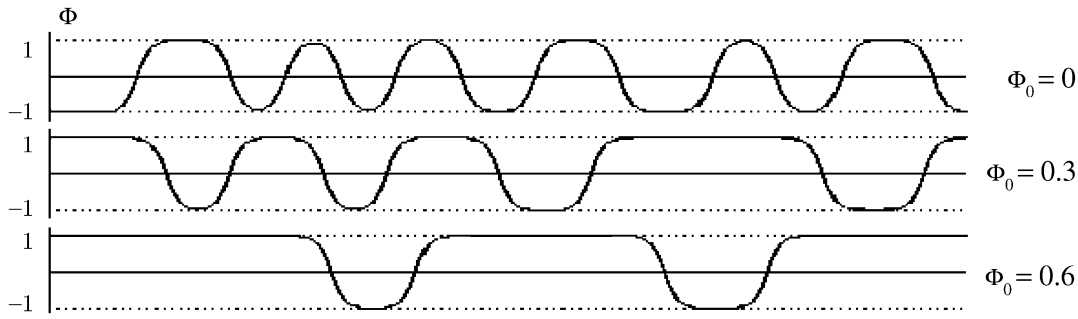

Fluid Dynamics, Pattern Formation, Fig. 25 Stationary solutions of the ID Cahn-Hilliard equation for several mean values Φ_0

The density of the free energy of a homogeneous solution reads

$$f(\Phi) = -\frac{\Phi^2}{2} + \frac{\Phi^4}{4} \tag{91}$$

and has its minima at $\Phi_m = \pm 1$. From Fig. 25 it becomes clear that the stationary pattern forming solutions are located between these two minima independently from the mean Φ_0. If the mean value is increased, the regions with $\Phi \approx 1$ grow at the cost of the regions with $\Phi \approx -1$ and vice versa. Taking (90) as a simple model for the phase transition from liquid to gas, the phase field defines the state of aggregation. The density can then be found from the linear relation

$$\rho\left(\vec{r},t\right) = \frac{1}{2}\left(\rho_f - \rho_g\right)\Phi\left(\vec{r},t\right) + \frac{1}{2}\left(\rho_f + \rho_g\right) \tag{92}$$

with ρ_g (ρ_f) as the density of the gaseous (liquid) state. Regions where $\Phi \approx -1$ are gaseous, those with $\Phi \approx +1$ liquid.

Equation (90) has no free parameters. On the other hand, the mean $\Phi_0 = \langle\Phi\rangle$ is a conserved quantity which influences the dynamics of pattern formation qualitatively and which can be considered as a control parameter. Integrating (92) over the volume, it turns out that Φ_0 is linked to the total mass M of the gas/liquid system

$$M = \frac{1}{2}\left(\rho_f - \rho_g\right)\Phi_0 \cdot V + \frac{1}{2}\left(\rho_f + \rho_g\right) \cdot V.$$

The stable homogeneous solutions $\Phi_0^2 > 1/3$ correspond to a pure gas phase ($\Phi_0 < 0$, small total mass), or to a pure liquid phase ($\Phi_0 > 0$, large total mass). In the unstable regime $\Phi_0^2 < 1/3$ the (homogeneous) system has a medium density; this corresponds either to an oversaturated vapor atmosphere ($\Phi_0 < 0$) or to a liquid with a temperature above its boiling point. In both cases, an infinitesimally small disturbance is sufficient to trigger pattern formation in the form of phase separation. In the first case, one observes drops in the gas atmosphere, in the latter, bubbles in the liquid. Figure 26 shows a numerical simulation of (90) in three dimensions.

The Fluid Density as Phase Field

Writing down an equation such as (87) and an expansion such as (88) seems to be rather ad hoc. However, for pure fluids it is evident to use the density itself as the phase field, if one is interested in the liquid/gas phase transition. Then, the continuity Eq. (2) may serve as a phase field equation in lieu of (87). Consequently, the fluid can no longer be considered incompressible.

The Model The Navier–Stokes equations for a compressible fluid (14) must be extended by a force term coming from spatial variations of the phase field (density). They read (Borcia and Bestehorn 2007; Jasnow and Vinals 1996)

$$\rho\left[\partial_t\vec{v} + \left(\vec{v}\cdot\nabla\right)\vec{v}\right] = -\mathrm{grad}\,p + \vec{f} + \eta\Delta\vec{v} + \left(\zeta + \frac{\eta}{3}\right)\mathrm{grad}\,\mathrm{div}\,\vec{v} + \mathcal{K}\rho\,\mathrm{grad}\,\Delta\rho. \tag{93}$$

The extra term at the end of (93) was first used by Korteweg in 1901 and is sometimes called Korteweg stress (Korteweg 1901). For (93) we assumed constant material parameters η, ζ and $\mathcal{K}$. Using the methods of thermodynamics, the pressure is related to the free energy density f (Anderson and Mc Fadden 1997; Davis and Scriven 1982)

$$p(\rho) = \rho\frac{\partial f(\rho)}{\partial\rho} - f(\rho) \tag{94}$$

and the free energy as a functional of ρ reads

$$F[\rho] = \int_V \mathrm{d}^3\vec{r}\left[\frac{\mathcal{K}}{2}(\nabla\rho)^2 + f(\rho)\right], \tag{95}$$

according to (88). Equations (93) with (94) and (2) form a closed system for the variables $\vec{v}$ and ρ. Wetting properties and contact angles at the walls depend on the boundary conditions $\rho = \rho_w$ along the wall (Pismen and Pomeau 2000). The choice $\rho_w = \rho_f$ corresponds to a completely wetting (hydrophilic) material, $\rho_w = \rho_g$ to a non-wetting (hydrophobic) boundary. The boundary condition for $\vec{v}$ can either be no-slip (along a wall), no flux, or periodic. It is straightforward to include evaporation and condensation effects into the model, which is studied in (Borcia and Bestehorn 2005).

Note that now the free energy (95) is not needed for determining the evolution of the

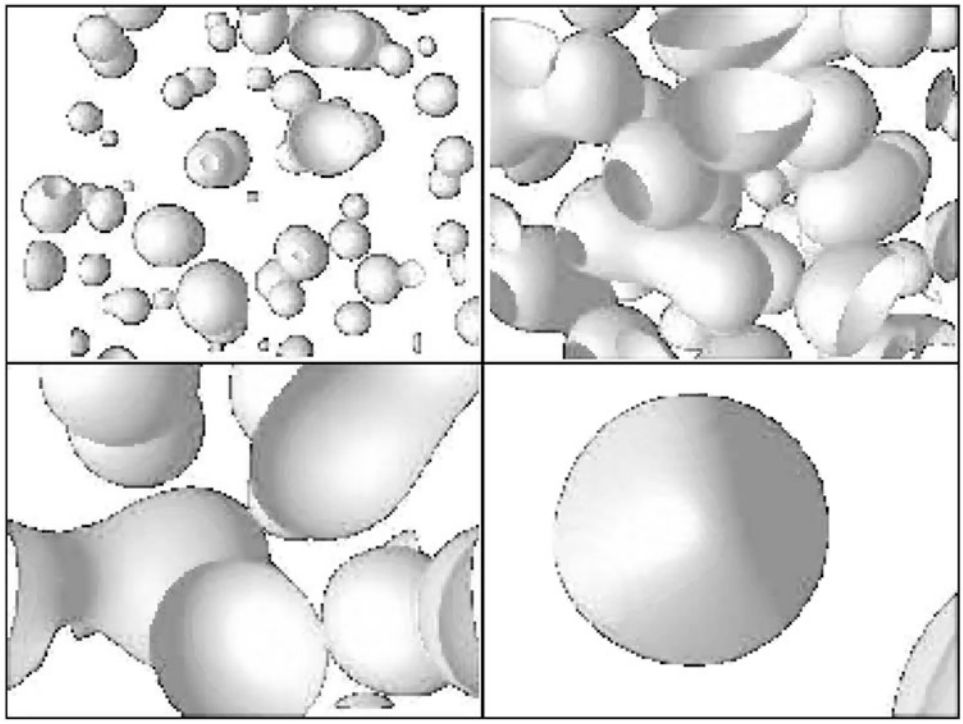

Fluid Dynamics, Pattern Formation, Fig. 26 Numerical solution of the Cahn-Hilliard Eq. (90) in three room dimensions. The time series (*top left to bottom right*) shows how liquid drops are formed in an oversaturated gas atmosphere. Finally they merge to one big drop by coarsening, a typical dynamic for a type II instability (from (Bestehorn 2006))

phase field by (*ad-hoc*) gradient dynamics. However, it can be shown that the free energy decreases monotonically in time.

Results Again, we wish to consider the formation of one state of aggregation on the background of the other. To account for the two stable states, liquid and gaseous, we take (for sake of simplicity we assume $\rho_g \approx 0$)

$$f(\rho) = \gamma\rho^2\left(\rho - \rho_f\right)^2. \qquad (96)$$

where y is a positive material constant. In Fig. 27 we show results of the breakup of a flat liquid film aligned along a rigid bottom plate. The layer is inclined by an angle φ and under vertical gravitation. Thus, an external force density of the form

$$\vec{f} = \rho g \begin{pmatrix} \sin\varphi \\ -\cos\varphi \end{pmatrix}$$

occurs in (93). The bottom material is assumed to be partially wetting ($\rho_w = 0.5\rho_f$) and the initial film is unstable under these conditions. Periodic disturbances grow along the fluid's surface. After rupture, bubbles separate and travel from left to right due to downhill force. Figure 28 shows final states of a sliding drop for two boundary values ρ_w. Clearly, the contact angles are different (Borcia et al. 2008a).

The phase field description goes far beyond the one based on the thin film equation of Section "Thin Films", since there the treatment was restricted to small contact angles and rupture was excluded from the beginning.

Future Directions

There is a huge number of applications in science, industry, and technology where the methods and models outlined in the present article can be used and developed further. In the field of patterns not

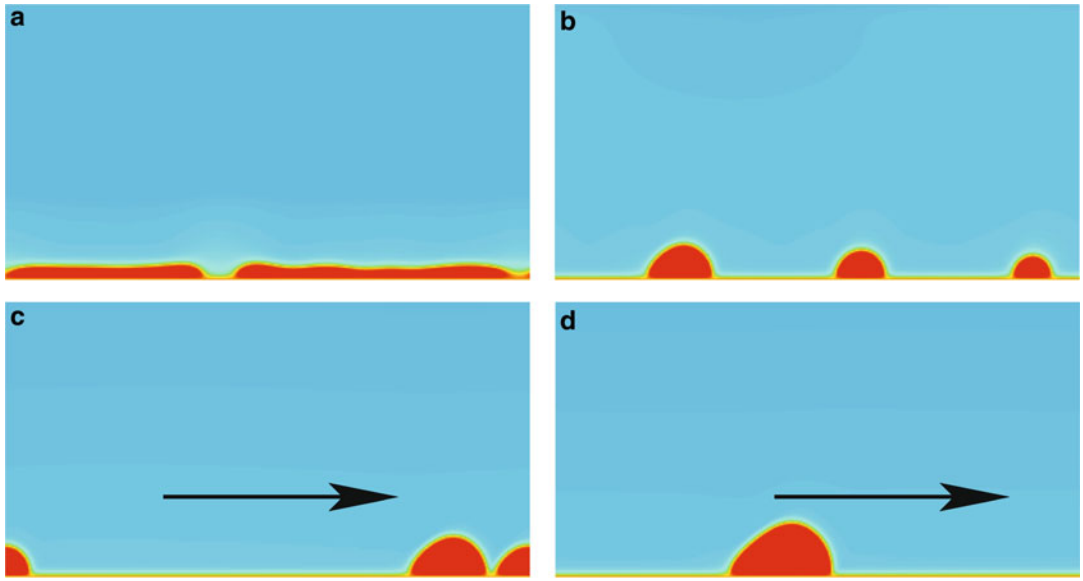

Fluid Dynamics, Pattern Formation, Fig. 27 Transition from a flat unstable liquid layer to a drop running down on an inclined substrate (arrows) under gravity effects. Numerical simulation (Borcia et al. 2008a) of (93) with (96) and the material parameters for water/vapor from (Burelbach et al. 1988) and $\rho_w = 0.5\rho_f$

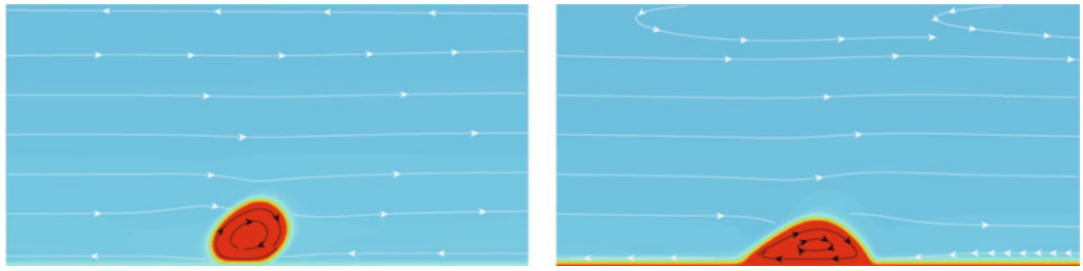

Fluid Dynamics, Pattern Formation, Fig. 28 Two final states showing a drop sliding down the inclined substrate with $\rho_w = 0.1\rho_f$ (left, almost hydrophobic) and $\rho_w = 0.8\rho_f$ (*right,* almost hydrophilic). The flow in the gas and in the liquid is indicated by *small arrows* (Borcia et al. 2008b)

formed by self-organized processes, but rather by external events such as tidal waves, storm surges or Tsunamis, a reduced and simplified description as discussed in Sections "Surface Waves" and "Order Parameter Equations" should allow for a better understanding of the underlying mechanisms and their effects. Highly involved problems, as for instance the flow, temperature, and concentration fields inside a combustion cell, could be tackled by such models, extended in a suitable way.

Self-organized fluid patterns (Section "Instabilities") are the focus of attention in many actual fields of quite different disciplines and scales. The conditions that lead to the creation and stabilization of hurricanes are not yet completely known. The rather high probability of the occurrence of freak waves in the open sea still waits for an explanation. On a planetary scale, convection problems are encountered in the interior of planets and stars and may give rise to the spontaneous formation of a magnetic field. Another problem of great interest for the geophysicist is that of a fluid (such as oil) in a porous medium. The equations for that case differ only a little from that discussed in Section "The Basic Equations of Fluid Dynamics" and could therefore be treated in the same spirit.

Understanding the mechanisms responsible for pattern formation can also help to control systems to avoid the occurrence of spatial patterns. In this way, the quality of products obtained from industrial processes, such as coating or solidification (crystal growth), might be improved.

On the micro-scale, fluid problems in general ruled by the Stokes equations discussed in Section "Conserved Order Parameter Fields" form a major issue, founding the new discipline of micro-fluidics. But even on the nanoscale, there are new applications in view. The self-organized growth of structures could be a promising tool in the conception and construction of nano-circuits.

An extension of the treatment to complex fluids such as mixtures and emulsions, or to non-Newtonian fluids using the phase field approach (Section "Conserved Order Parameter Fields"), is desirable. These fluids are important for biological applications.

Bibliography

Primary Literature

Abramowitz M, Stegun IA (1965) Handbook of mathematical functions. Dover, New York

Anderson DM, Mc Fadden GB (1997) A diffuse-interface description of internal waves in a near-critical fluid. Phys Fluids 9:1870–1879

Aranson IS, Kramer L (2002) The world of the complex Ginzbur–Landau equation. Rev Mod Phys 74:99–143

Argyris JH, Faust G, Haase M (1994) An exploration of chaos: an introduction for natural scientists and engineers. North-Holland, Amsterdam

Bénard H (1901) Les tourbillons cellulaires dans une nappe liquide. Ann Chim Phys 23:62–143

Bestehorn M (1993) Phase and amplitude instabilities for Bénard–Marangoni convection in fluid layers with large aspect ratio. Phys Rev 48:3622–3634

Bestehorn M (1996) Square patterns in Bénard–Marangoni convection. Phys Rev Lett 76:46–49

Bestehorn M (2006) Hydrodynamik und Strukturbildung. Springer, Berlin

Bestehorn M (2007) Convection in thick and thin fluid layers with a free interface. Eur Phys J Spec Top 146:391–405

Bestehorn M, Colinet P (2000) Bénard–Marangoni-convection of a binary mixture as an example of an oscillatory bifurcation under strong symmetry-breaking effects. Phys D 145:84

Bestehorn M, Friedrich R (1999) Rotationally invariant order parameter equations for natural patterns in non-equilibrium systems. Phys Rev E 59:2642–2652

Bestehorn M, Haken H (1983) A calculation of transient solutions describing roll and hexagon formation in the convection instability. Phys Lett A 99:265–268

Bestehorn M, Haken H (1990) Traveling waves and pulses in a two-dimensional large-aspect-ratio system. Phys Rev A 42:7195–7203

Bestehorn M, Neuffer K (2001) Surface patterns of laterally extended thin liquid films in three dimensions. Phys Rev Lett 87:046101

Bestehorn M, Pérez-García C (1992) Study of a model of thermal convection in cylindrical containers. Phys D 61:67–76

Bestehorn M, Neufeld M, Friedrich R, Haken H (1994) Comment on spiral-pattern formation in Rayleigh–Bénard convection. Phys Rev E 50:625

Bestehorn M, Pototsky A, Thiele U (2003) 3D Large scale Marangoni convection in liquid films. EurPhys J B 33:457

Block MJ (1956) Surface tension as the cause of Bénard cells. Nat (London) 176:650–651

Bodenschatz E, Pesch W, Ahlers G (2000) Recent developments in Rayleigh–Bénard convection. Annu Rev Fluid Mech 32: 709–778

Borcia R, Bestehorn M (2005) Phase-filed simulations for evaporation with convection in liquid-vapor systems. Eur Phys J B 44:101–108

Borcia R, Bestehorn M (2007) Phase-field simulations for drops and bubbles. Phys Rev E 75:056309

Borcia R, Borcia I, Bestehorn M (2008a) Phys Rev E (submitted)

Borcia R, Borcia I, Bestehorn M (2008b) Static and dynamic contact angles. Eur Phys J Spec Top (in print)

Burelbach JP, Bankoff SG, Davis SH (1988) Nonlinear stability of evaporating/condensing liquid films. J Fluid Mech 195:463

Busse FH (1967) The stability of finite amplitude cellular convection. J Fluid Mech 30:625–649

Busse FH (1989) In: Peltier WR (ed) Fundamentals of thermal convection. Taylor, 23–95

Busse FH, Frick H (1985) Square-pattern convection in fluids with strongly temperature-dependent viscosity. J Fluid Mech 150:451–465

Busse FH, Riahi N (1980) Nonlinear convection in a layer with nearly insulating boundaries. J Fluid Mech 96:243–256

Cahn JW, Hilliard JE (1958) Free energy of a nonuniform system. J Chem Phys 28:258–267

Callen HB (1985) Thermodynamics and an introduction to thermostatistics. Wiley, New York

Castets V, Dulos E, Boissonade J, De Kepper P (1990) Experimental evidence of a sustained standing Turing-type nonequilibrium chemical pattern. Phys Rev Lett 64:2953–2956

Chandrasekhar S (1961) Hydrodynamic and hydromagnetic stability. Dover, New York

Cohen IM, Kundu PK (2004) Fluid mechanics. Academic, Amsterdam

Colinet P, Legros JC, Velarde MG (2001) Nonlinear dynamics of surface tension driven instabilities. Wiley, Berlin

Cross MC (1988) Theoretical methods in pattern formation in physics, chemistry and biology. In:Garrido L (ed) Far from equilibrium phase transitions. Springer, Berlin
Cross MC, Hohenberg PC (1993) Pattern formation outside of equilibrium. Rev Mod Phys 65:851–1112
Davis HT, Scriven LE (1982) Stress and structures in fluid interfaces. Adv Chem Phys 49:357
de Gennes PG (1985) Wetting: statics and dynamics. Rev Mod Phys 57:827–863
Dean RG, Dalrymple RA (2000) Water wave mechanics for engineers and scientists. World Science, Singapore
Drazin PG, Johnson RS, Crighton DG (1989) Solitons: an introduction. Cambridge University Press, Cambridge
Eckert K, Bestehorn M, Thess A (1998) Square cells in surface tension driven Bénard convection: experiment and theory. J Fluid Mech 356:155–197
Faraday M (1831) On a peculiar class of acoustical figures and on certain forms assumed by groups of particles upon vibrating elastic surfaces. Philos Trans R Soc Lond 121:299
Getling AV (1998) Rayleigh–benard convection: structures and dynamics. World Scientific
Golovin AA, Nepomnyashchy AA, Pismen LM (1997) Nonlinear evolution and secondary instabilities of Marangoni convection. J Fluid Mech 341:317–341
Guckenheimer J, Holmes P (2002) Nonlinear oscillations, dynamical systems, and bifurcations of vector fields. Springer, Berlin
Haken H (1975) Cooperative phenomena in systems far from thermal equilibrium and in nonphysical systems. Rev Mod Phys 47:67–121
Haken H (1983) Advanced synergetics: instability hierarchies of self-organizing systems and devices. Springer, Berlin
Haken H (2004) Synergetics introduction and advanced topics. Springer, Berlin
Hardy W (1919) The spreading of fluids on glass. Philos Mag 38:49–55
Hohenberg PC, Halperin BI (1977) Theory of dynamic critical phenomena. Rev Mod Phys 49:435–447
Israelachvili JN (1992) Intermolecular and surface forces. Academic, London
Jasnow D, Vinals J (1996) Coarse-grained description of thermo-capillary flow. Phys Fluids 8:660–669
Korteweg DJ (1901) Sur la forme que prennent les équation du mouvements des fluides. Arch Néerl Sci Exact Nat Ser II 6:1
Koschmieder EL (1993) Bénard cells and Taylor vortices. Cambridge University Press, Cambridge
Lai WM, Rubin D, Krempl E (1993) Introduction to continuum mechanics. Pergamon, Oxford
Landau LD, Lifshitz EM (1996) Statistical physics. In: Course of theoretical physics, 5. Heinemann, Butterworth
Landau LD, Lifshitz EM (2004) Fluid dynamics. In: Course of theoretical physics, 6. Heinemann, Butterworth
Langer JS (1980) Instabilities and pattern formation in crystal growth. Rev Mod Phys 52:1–28
Lorenz EN (1963) Deterministic nonperiodic flow. J Atmos Sci 20:130–141
Morris SW, Bodenschatz E, Cannell DS, Ahlers G (1993) Spiral defect chaos in large aspect ratio Rayleigh–Bénard convection. Phys Rev Lett 71:2026–2029
Moses E, Steinberg V (1986) Competing patterns in a convective binary mixture. Phys Rev Lett 57:2018–2021
Murray JD (1993) Mathematical biology. Springer, Berlin
Nekorkin VI, Velarde MG (2002) Synergetic phenomena in active lattices. Patterns, waves, solitons, chaos. Springer, Berlin
Nepomnyashchy AA, Velarde MG, Colinet P (2002) Interfacial phenomena and convection. Chapman & Hall, Boca Raton
Newell AC, Whitehead JA (1969) Finite bandwidth, finite amplitude convection. J Fluid Mech 38:279–303
Nitschke-Eckert K, Thess A (1995) Secondary instability in surface tension driven Bénard convection. Phys Rev E 52: 5772–5775
Ockendon H, Ockendon JR (1995) Viscous flow. Cambridge University Press, Cambridge
Oron A (2000) Nonlinear dynamics of three-dimensional longwave Marangoni instability in thin liquid films. Phys Fluids 12:1633–1645
Oron A, Davis SH, Bankoff SG (1997) Long-scale evolution of thin liquid films. Rev Mod Phys 69:931–980
Ouyang Q, Swinney HL (1991) Transition from a uniform state to hexagonal and striped Turing patterns. Nature 352:610–612
Palm E (1960) On the tendency towards hexagonal cells in steady convection. J Fluid Mech 19:183–192
Penrose R (1974) Role of aesthetics in pure and applied research. Bull Inst Math Appl 10:266
Pesch W (1996) Complex spatiotemporal convection patterns. Chaos 6:348–357
Pismen LM, Pomeau Y (2000) Disjoining potential and spreading of thin liquid layers in the diffuse-interface model coupled to hydrodynamics. Phys Rev E 62:2480–2492
Prigogine I, Levever R (1968) Symmetry breaking instabilities in dissipative systems II. J Chem Phys 48:1695–1700
Prigogine I, Nicolis G (1967) On symmetry-breaking instabilities in dissipative systems. J Chem Phys 46:3542–3550
Rayleigh Lord (1915) On convection currents in a horizontal layer of fluid. Philos Mag 32:462–468
Reiter G, Sharma A, Casoli A, David M-O, Khanna R, Auroy P (1999) Thin film instability induced by long-range forces. Langmuir 15:2551–2558
Schatz MF, Neitzel GP (2001) Experiments on thermocapillary instabilities. Annu Rev Fluid Mech 33:93–127
Schatz MF, Van Hook SJ, Mc Cormick WD, Swift JB, Swinney HL (1999) Time-independent square patterns in surface-tension-driven Bénard convection. Phys Fluids 11:2577–2582
Scheid B, Oron A, Colinet P, Thiele U, Legros JC (2002) Nonlinear evolution of nonuniformly heated falling liquid films. Phys Fluids 14:4130–4151
Schwabe D (2006) Marangoni instabilities in small circular containers under microgravity. Exp Fluids 40:942–950

See the up to now 69 volumes of the Springer Series of Synergetics, especially the monographs by Haken H (1983) Synergetics. An introduction.; Advanced synergetics.; Information and self-organization (2006)
Seemann R, Herminghaus S, Jacobs K (2001) Dewetting patterns and molecular forces: a reconciliation. Phys Rev Lett 86:5534–5553
Sharma A, Khanna R (1998) Pattern formation in unstable thin liquid films. Phys Rev Lett 81:3463–3466
Sharma A, Khanna R (1999) Pattern formation in unstable thin liquid films under the influence of antagonistic short and long-range forces. J Chem Phys 110:4929–4936
Sparrow C (1982) The Lorenz equations. Springer, Berlin
Swift JB, Hohenberg PC (1977) Hydrodynamic fluctuations at the convective instability. Phys Rev A 15:319; Chem Phys 48:1695–1700
Turing AM (1952) The chemical basis of morphogenesis. Philos Trans R Soc Lond B237:37
Van Dyke M (1982) An album of fluid motion. Parabolic, Stanford
Van Oss CJ,Chaudhury MK, Good RJ (1988) Interfacial Lifshitz–van der Waals and polar interactions in macroscopic systems. Chem Rev 88:927–941
Vrij A (1966) Possible mechanism for the spontaneous rupture of thin, free liquid films. Disc Faraday Soc 42:23–33

Books and Reviews

Emmerich H (2003) The diffusive interface approach in material science. Springer, Berlin
Fletcher CAJ (1988) Computational techniques for fluid dynamics, 1,2. Springer, Berlin
Manneville P (1990) Dissipative structures and weak turbulence. Academic, London
Pismen LM (2006) Patterns and interfaces in dissipative dynamics. Springer, Berlin
Platten JK, Legros JC (1984) Convection in liquids. Springer, Berlin
Schlichting H, Gersten K (2000) Boundary-layer theory. Springer, Berlin
Simanovskii IB, Nepomnyashchy AA (1993) Convective instabilities in systems with interface. Gordon Preach, Yverdon